Elucidation of the membrane and metal binding interface of Nup214/Nup88 sub complex of the nuclear pore complex

A Thesis

submitted to

Indian Institute of Science Education and Research Pune in partial fulfilment of the requirements for the BS-MS Dual Degree Programme

by

Anish Pandey

Indian Institute of Science Education and Research Pune

Dr. Homi Bhabha Road,

Pashan, Pune 411008, INDIA.

Date: April 2025

Under the guidance of

Supervisor: Dr. Radha Chauhan,

National Centre for Cell Science

From May 2024 to Mar 2025

INDIAN INSTITUTE OF SCIENCE EDUCATION AND RESEARCH PUNE

Certificate

This is to certify that this dissertation entitled “Elucidation the membrane and metal binding interface of Nup214/Nup88 sub complex of the nuclear pore complex” towards the partial fulfilment of the BS-MS dual degree programme at the Indian Institute of Science Education and Research, Pune represents study/work carried out by Anish Pandey at Indian Institute of Science Education and Research under the supervision of Dr Radha Chauhan, Scientist F, National Centre for Cell Science, during the academic year 2024-2025.

Dr Radha Chauhan
(Guide)

Committee:

Dr Radha Chauhan (Guide) 

Dr Gayathri Pananghat (TAC) 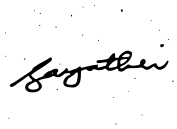

This thesis is dedicated to my family.

Declaration

I hereby declare that the matter embodied in the report entitled "Elucidation the membrane and metal binding interface of Nup214/Nup88 sub complex of the nuclear pore complex" are the results of the work carried out by me at the National Centre for Cell Science, under the supervision of Dr Radha Chauhan, and the same has not been submitted elsewhere for any other degree. Wherever others contribute, every effort is made to indicate this clearly, with due reference to the literature and acknowledgement of collaborative research and discussions.

Anish Pandey

20191055

Table of Contents

List of Tables

List of Figures

1. Abstract

The nuclear pore complex (NPC) is a large megadalton assembly that functions as an exclusive gateway between the nucleus and the cytoplasm, responsible for bi-directional nucleocytoplasmic transport. The NPC is composed of 32 to 34 different types of proteins known as nucleoporins (Nups) that are present in multiple copies (8, 16, 32, or up to 48). These Nups assemble together to form highly modular assembly structures that can range from ~60 to ~120 MDa in yeast and humans respectively. These Nups are found to be arranged in various subcomplexes like the cytoplasmic ring complex (CR), the inner ring complex (IR), the central transport channel (CTC), the nuclear ring complex (NR), and the Y-complex. Among them, the CR complex, containing the Nup88·Nup62·Nup214 complex is exclusively involved in mRNA transport, by virtue of its positioning over the CTC. Understanding the interactions of these Nups with each other as well as the nuclear membrane is vital to understand assembly as well as functioning of the NPC. Central to the interactions are the beta-propellor (**β**) domains of Nup88 and Nup214. Here we report purification of these two subunits *in vitro* and attempts for purification of their complex. We further performed *in silico* analysis of these subunits to determine their membrane binding propensity, interaction strength, as well as metal binding potential.

2. Acknowledgments

I would like to sincerely thank my supervisor, Dr. Radha Chauhan, for giving me the opportunity to work under her guidance and carry out this project. It was a pleasure to learn from her.

I would also like to extend my thanks to Dr. Sunil Bhagwat, Director of IISER Pune, and Dr. Sharmila Bapat, Director of NCCS for providing facilities to carry out this project.

I am greatly thankful to Dr. Gayathri Pananghat for her role as advisor in this project. Her insights as well as support were vital for the completion of this project.

I would like to extend my sincere thanks to Mr. Bheem Singh Bhandari, who was my immediate mentor in the lab. His support and guidance greatly helped me in completing this project. I would also like to thank my lab seniors Dr. Krishnakant Gupta, Ms. Aswathy LB, Mr. Krishna Mondal, Mr. Vyankatesh Rajamane and Mr. Subhajit Das for sharing their knowledge and helping me throughout my work.

Special thanks to my lab seniors Ms. Jyotsana Singh and Mr. Monty Vijayvargiya. I will always cherish the conversations I had with them. A special mention to my friends Santam Saha and AK Balaji. They were always ready to provide any help or support I needed. I am also grateful to everyone at IISER and NCCS who contributed to this project directly or indirectly.

Lastly, I would like to thank my father Mr. Anil Pandey, mother Mrs. Shalini Pandey, and my younger brother Master Ansh Pandey. Their prayers, love, support and sacrifice mean the world to me, and without them, I would not be who I am today.

Anish Pandey

3. Contributions

Contributor name	Contributor role
Dr Radha Chauhan	Conceptualization Ideas
Dr Radha Chauhan, Anish Pandey	Methodology
-	Software
Anish Pandey	Validation
Anish Pandey	Formal analysis
Anish Pandey	Investigation
Dr Radha Chauhan	Resources
Anish Pandey	Data Curation
Anish Pandey	Writing - original draft preparation
Anish Pandey, Dr Radha Chauhan	Writing - review and editing
Anish Pandey	Visualization
Dr Radha Chauhan	Supervision
Dr Radha Chauhan	Project administration
Dr Radha Chauhan	Funding acquisition

Chapter 1 Introduction

1.1 The nucleus, nuclear envelope and the nuclear pore complex

The nucleus, often regarded as the command center of the eukaryotic cell, is a marvel of biological architecture and function, seamlessly integrating the nuclear envelope and the nuclear pore complex (NPC) into a cohesive system that governs cellular life (Hetzer, 2010). Enclosed within the nuclear envelope, a double-membraned barrier composed of an inner and outer nuclear membrane, the nucleus not only houses the cell's genetic material but also orchestrates the intricate processes of gene expression, DNA replication, and RNA processing. The inner nuclear membrane is reinforced by the nuclear lamina, a protein meshwork that provides structural stability and plays a pivotal role in chromatin organization and gene regulation, while the outer nuclear membrane is continuous with the endoplasmic reticulum (ER), creating a direct link between the nucleus and the broader endomembrane system (Hetzer, 2010). This continuity is not merely structural but functional, enabling coordinated responses to cellular stress and signaling events, and underscoring the nucleus's role as a dynamic entity rather than a static repository of DNA. The nuclear envelope, however, is not an impermeable fortress; it is punctuated by nuclear pores, each embedded with an NPC, a colossal and highly sophisticated protein complex that serves as the gateway for molecular traffic between the nucleus and the cytoplasm (Alber et al., 2007). The NPC, composed of multiple copies of 32 to 34 different proteins known as nucleoporins (Nups), is one of the most intricate molecular machines in the cell, capable of selectively regulating the bidirectional transport of molecules (Wente & Rout, 2010). Small molecules and ions can diffuse freely through the NPC, but larger molecules, such as proteins and RNA, require active transport, a process mediated by specific recognition mechanisms. For instance, nuclear localization signals (NLS) on proteins are recognized by importins, which facilitate their translocation into the nucleus, while nuclear export signals (NES) are recognized by exportins, guiding proteins and RNA out of the nucleus (Wente & Rout, 2010). This selectivity ensures that the nucleus maintains precise control over its internal environment, a necessity for proper cellular function. Beyond its role as a gatekeeper, the NPC is a dynamic and adaptable structure, with its composition and function varying depending on cell type, developmental stage, and environmental conditions (Wente & Rout, 2010). This plasticity allows the cell to fine-tune nucleocytoplasmic transport in response to changing demands, such as during cell division,

differentiation, or stress responses. Moreover, the NPC has been implicated in a variety of regulatory processes beyond transport, including gene expression, chromatin organization, and DNA repair, highlighting its multifaceted role in cellular physiology (Alber et al., 2007). Together, the nuclear envelope and the NPC form a highly integrated system that underpins the cell's ability to maintain genomic integrity, regulate gene expression, and respond to its environment. The nuclear envelope provides both a protective barrier and a structural framework, while the NPC ensures the precise and regulated exchange of molecules essential for cellular function (Hetzer, 2010).

1.2 Structure of the NPC

The NPC exhibits an intricate eightfold rotational symmetry around its central axis, with a pseudo-twofold symmetry perpendicular to the nuclear envelope plane, reflecting its modular and repetitive architecture (Lin et al.,2019). This symmetrical organization is critical for its function as a bidirectional transport channel and structural scaffold. At the core of the NPC lies the central scaffold, a cylindrical framework composed of stacked rings that form the primary structural backbone. The scaffold is divided into three main layers: the inner ring, the outer rings (cytoplasmic and nuclear), and the membrane ring. The inner ring, composed of Nup155, Nup205, and Nup188, Nup93 and Nup35 forms a rigid lattice that stabilizes the entire complex (Huang et al.,2022). This lattice is flanked by the cytoplasmic and nuclear rings, which are structurally similar but functionally distinct. The cytoplasmic ring, enriched with Nup358, Nup214 and Nup88, serves as a docking site for cytoplasmic transport factors (Stuwe et al.,2022). Nup214, in particular, is known for its role in mediating the export of mRNAs and proteins, while Nup88, often found in complex with Nup214, contributes to the structural integrity and regulatory functions of the cytoplasmic ring (Hutten et al., 2006; Li et al., 2021). On the nuclear side, the ring features Nup153 and Tpr, which interact with nuclear transport machinery and participate in chromatin organization (Vollmer et al., 2012). The membrane ring, embedded within the nuclear envelope, anchors the NPC to the lipid bilayer via transmembrane Nups such as GP210 and POM121. These Nups not only provide structural stability but also facilitate the curvature of the nuclear envelope around the NPC (Anotnin et al.,2008). The membrane ring's integration with the inner and outer rings ensures the NPC's structural continuity and mechanical resilience, allowing it to withstand the forces exerted during nucleocytoplasmic transport. One of the most distinctive features of the

NPC is its permeability barrier, formed by intrinsically disordered regions (IDRs) of FG-repeat-containing Nups. These Nups, including Nup62, Nup98, and Nup54, project into the central transport channel, creating a dynamic hydrogel-like meshwork (Frey et al.,2006). The FG repeats interact transiently with nuclear transport receptors, enabling the selective passage of cargoes while excluding untagged macromolecules. This disordered yet functional domain exemplifies the interplay between structural rigidity and dynamic flexibility in the NPC's architecture. Recent advances in cryo-electron tomography (cryo-ET) and integrative modelling have provided near-atomic resolution insights into the NPC's structure. For instance, the inner ring's Y-complex, a conserved structural module composed of multiple Nups, has been visualized in exquisite detail, revealing its role in nucleating NPC assembly (Kelly et al.,2015; von Appen et al.,2015). Similarly, the spatial arrangement of FG-Nups within the central channel has been mapped, shedding light on the molecular basis of selective transport (Ma et al.,2016). These structural studies have also highlighted the conformational plasticity of the NPC, which undergoes dynamic rearrangements to accommodate cargoes of varying sizes and shapes (Beck et al.,2022).

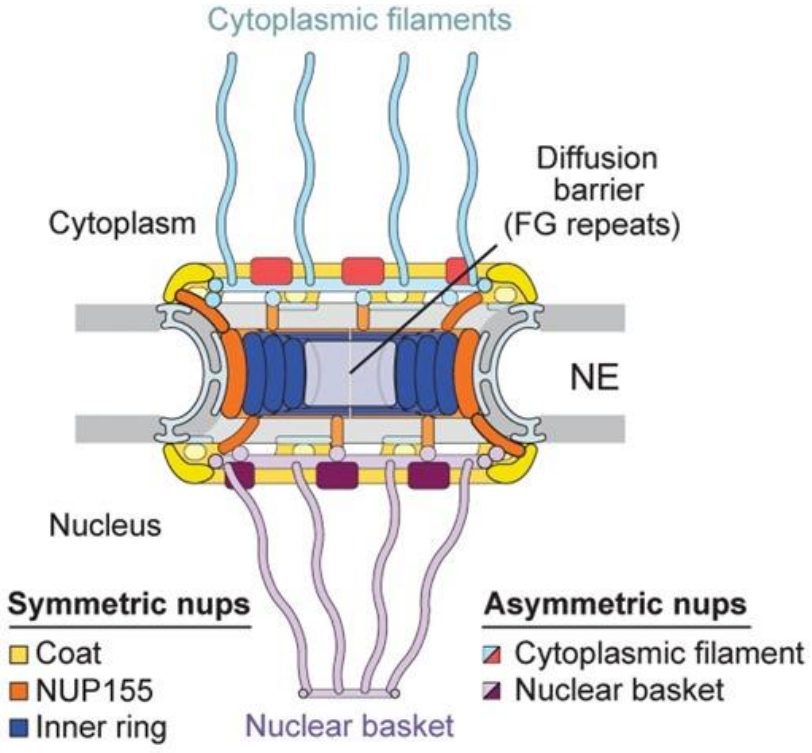

Figure1. Structure of the Nuclear Pore Complex (Bley et. al. Science 2022)

1.3 Nup88 and Nup214

The Nup214-Nup88 complex is a critical component of the cytoplasmic face of the nuclear pore complex (NPC), playing essential roles in nucleocytoplasmic transport, mRNA export, and the regulation of specific signalling pathways. Structurally, this complex is anchored to the cytoplasmic ring of the NPC and is composed of two major nucleoporins: Nup214 (also known as CAN) and Nup88. Both proteins are evolutionarily conserved and exhibit distinct structural features that enable their functional versatility within the NPC. Nup214 is a large, multidomain protein characterized by an N-terminal β-propeller domain, a central coiled-coil region, and a C-terminal FG-repeat domain. The β-propeller domain, composed of seven blades, serves as a binding platform for various transport factors, including the export receptor CRM1 (also known as XPO1) (Napetschnig et al.,2007). The coiled-coil region mediates the interaction with Nup88, forming a stable heterodimeric complex that is essential for the structural integrity of the cytoplasmic ring (Bernard et al.,2022). The C-terminal FG-repeat domain of Nup214 projects into the central transport channel, where it contributes to the NPC's permeability barrier and facilitates the transient binding of nuclear transport receptors (Port et al.,2015). Structural studies, including X-ray crystallography and cryo-electron microscopy (cryo-EM), have revealed that the β-propeller domain of Nup214 adopts a canonical seven-bladed fold, while the coiled-coil region forms an extended helical bundle that interacts with Nup88 (Bono et al.,2010). Nup88, in contrast, is a smaller protein that primarily functions as a stabilizing partner for Nup214. It consists of an N-terminal β-propeller domain and a C-terminal coiled coil domain. The β-propeller domain of Nup88 is structurally similar to that of Nup214, though it lacks the extensive FG repeats found in the latter. Instead, Nup88's α-helical domain is responsible for binding to the coiled-coil region of Nup214, forming a tight heterodimeric complex. Notably, structural data have shown that the β-propeller domains of Nup214 and Nup88 interact directly with each other, forming a compact interface that stabilizes the complex. This interaction is mediated by complementary surfaces on the β-propeller domains, which align in a head-to-head configuration, enhancing the overall stability of the Nup214-Nup88 complex (Kelly et al.,2015). This head-to-head arrangement of the β-propeller domains is a distinctive feature of the complex and is critical for its structural and functional integrity within the NPC (Schwartz et al.,2015). The Nup214-Nup88 complex is not only a structural entity but also a functional hub within the NPC. Nup214's FG-repeat domain interacts with CRM1, facilitating the export of proteins and ribonucleoprotein complexes out of the

nucleus (Hutten et al., 2006). This interaction is regulated by the small GTPase Ran, which binds to CRM1 and modulates its affinity for cargoes. Structural studies have shown that the β-propeller domain of Nup214 directly binds to CRM1, providing a docking site for export complexes as they exit the nucleus (Monecke et al.,2009). Nup88, while less directly involved in transport, plays a crucial role in stabilizing Nup214 and modulating its function. The Nup214-Nup88 complex has been shown to form higher-order oligomers, which may contribute to the structural organization of the cytoplasmic ring (Madheshiya et al.,2022). Cryo-EM studies have revealed that the complex is positioned at the periphery of the cytoplasmic filaments, where it interacts with other nucleoporins such as Nup358 (also known as RanBP2) (Hutten et al.,2016). This positioning allows the Nup214-Nup88 complex to serve as a nexus for the assembly of transport complexes and the regulation of nucleocytoplasmic transport.

The structural characterization of individual β-propeller domains within the NPC has been achieved to varying extents. For instance, the N-terminal domain of human Nup214 has been crystallized, revealing a seven-bladed β-propeller structure. This domain is followed by a 30-residue C-terminal extension that folds back onto the β-propeller, potentially playing a role in NPC assembly (Napetschnig et al., 2007). However, the high-resolution structure of human Nup88's β-propeller domain has not been determined. Sequence homology and structural predictions, postulate that it adopts a similar seven-bladed β-propeller configuration. The interaction between Nup214 and Nup88 is well-documented, primarily mediated through their coiled-coil domains. Co-immunoprecipitation experiments have demonstrated that both wild-type and NES-mutant versions of Nup214 can co-precipitate endogenous Nup88, indicating that residues beyond the NES motif facilitate this interaction (Hamed et al.,2021). Additionally, *in vitro* studies have shown that the coiled-coil regions of Nup214 (residues 693-976) interact stably with the coiled-coil regions of Nup88 (residues 517-742) and Nup62 (residues 322-525), suggesting a cooperative assembly mechanism within the NPC (Madhesiya et al., 2022). Despite these findings, the exact structural arrangement of the Nup214-Nup88 β-propeller domain complex remains elusive. Structural studies on the yeast Nup82 complex, which is homologous to the human Nup88-Nup214 complex, have provided some insights. The yeast Nup82 complex forms an asymmetric structure with a dynamic dimeric array of subunits, integrating both β-propeller and α-helical domains (Gaik et al., 2015). However, it is vital that similar studies be carried out for the human variants of these two β-propeller domains. The interaction of Nups with the nuclear envelope membrane is critical for

NPC assembly and stability. While certain nucleoporins, such as Nup53 and Nup155, have been shown to possess membrane-binding domains that facilitate their association with the inner nuclear membrane via their β-propeller domains, the membrane-binding potential of Nup214 and Nup88 remains largely unexplored (Vollmer et al.,2012; Vollmer et al.,2015). The absence of a resolved structure for the Nup214-Nup88 β-propeller domain complex presents a significant gap in our understanding of NPC architecture and function. Elucidating this structure would provide insights into the mechanistic aspects of nucleocytoplasmic transport and the role of these nucleoporins in NPC assembly. Furthermore, investigating the membrane-binding potential of Nup214 and Nup88 could unveil novel aspects of NPC-membrane interactions.

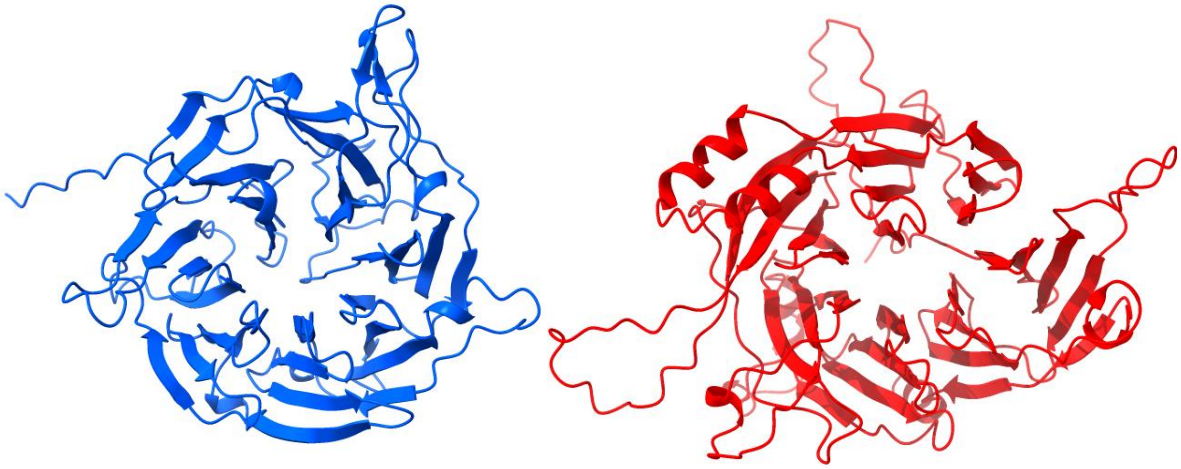

Figure2. Structure of the β-propeller domains of hNup214 and hNup88

This study focused on the β-propeller domains of human Nup214 and Nup88. *In vitro* expression and purification of these domains was attempted, alongside reconstitution of the complex formed by the interaction of these domains. Furthermore, *in silico* analysis of the individual β-propeller domains shed light on the membrane binding potential of these proteins. Furthermore, this study also focused on identifying metal binding pockets in the β-propeller domain of human Nup214.

Chapter 2 Materials and Methods

2.1 Constructs used for purification

For the purpose of this study, two constructs were previously cloned in the lab. The gene encoding the β-propeller domain of hNup214 was cloned into a pGEX4T1 vector, which contains an N-terminal Glutathione S-Transferase (GST) tag. The β-propeller domain lies between residue number 1 to 410 of the full length hNup214. The molecular weight of the protein expressing from the pGEX4T1 vector, along with the N-terminal GST tag is 71.2 kDa with a calculated pI of 4.98.

The gene encoding the β-propeller domain of hNup88 was cloned into a pET28a vector, which contains an N-terminal 6xHistidine tag. The β-propeller domain lies between residue number 51 to 498 of the full length hNup88. The molecular weight of the protein expressing from the pET28a vector, along with the N-terminal 6xHis tag is 50.2 kDa with a calculated pI of 5.10.

2.2 Expression of proteins

Competent *E. coli* BL21(DE3) RIL cells were transformed using either pGEX4T1 or pET28a vectors containing hNup214β or hNup88β genes respectively via heat shock method. Precultures were prepared by single colony inoculation of *E. coli* BL21(DE3) RIL cells containing vector with gene or interest and incubated for 12hrs at 37°C in a shaking incubator at 180 rpm. LB containing 100 ug/mL Ampicillin in case of pGEX4T1 vector, or 50 µg/mL Kanamycin in case of pET28a vector, along with 35 µg/mL Chloramphenicol was inoculated with 1% preculture, and bacteria were grown at 37°C and 180 rpm until $O.D._{600}$ reached between 0.6-0.8. The grown culture was then induced with 0.45mM isopropyl β-D-1-thiogalactopyranoside (IPTG). Post induction times were optimized further (see Results). Cells were then harvested by centrifuging at 5000 rpm for 10 minutes at 4°C. They were either processed immediately, or were stored at -80°C.

2.3 Purification of proteins

The initial purification protocol was adapted from an existing protocol in the lab. The lysis buffer used is labelled lysis buffer 1, and its components listed in the table below.

Tris HCl pH 8	**20 mM**
NaCl	**250 mM**
β-Me	**5 mM**
PMSF	**1 mM**
Glycerol	**2 % v/v**
DDM	**1 % v/v**

Table 1 Components of lysis buffer 1. pH was set to 8.

Cells were resuspended in lysis buffer and were sonicated on ice at an amplitude of 35Hz for 18 cycles, with each cycle lasting 10s and time between each cycle being 20s. Following this, the lysate was centrifuged at 17,000 rpm for 1hr at 4°C. The supernatant was then bound against beads (Ni-NTA for His-tagged protein, GST for GST tagged protein) for 1hr in the case of Ni-NTA beads, or 3hrs for GST beads. After bead binding, beads were washed with 40 CV (bead volume) of wash buffer, the components of which are shown in the table below.

Protein was then eluted by incubating beads with elution buffer, the components for which are shown in the table below, for 15min per elution. All steps were carried out at 4°C.

Samples were collected at each stage to run in a 10% SDS-PAGE gel.

Following initial purifications, 1% DDM, which was being used in the lysis buffer, was replaced by 1% Triton X-100. This was labelled lysis buffer 2.

Tris HCl pH 8	20mM
NaCl	250 mM
β-Me	5 mM
Imidazole*	35 mM
Glycerol	2 % v/v
DDM	0.1 mM

Tris HCl pH 8	20mM
NaCl	250 mM
β-Me	5 mM
Imidazole*	300 mM
Glycerol	1 % v/v
DDM	0.1 mM
Reduced Glutathione^	10 mM

Table 2 and 3 Components of Wash and Elution buffers. pH was set to 8.

^ - Component only used in GST purification. * - Component only used in Ni-NTA purification.

Reagents	Volume (mL)
Resolving gel	
Distilled water	2.95
1.5 M Tris HCl (pH 8.8)	1.9
10% SDS	0.075
Acrylamide	2.5
10% Ammonium persulfate	0.075
TEMED	0.005
Stacking gel	
Distilled water	1.35
1 M Tris HCl (pH 6.8)	0.25
10% SDS	0.02
Acrylamide	0.335
10% Ammonium persulfate	0.02
TEMED	0.005

Table 4 Components of 10% SDS-PAGE gel

2.5 Size Exclusion Chromatography

Elutions were concentrated to desired concentration using a 30 kDa centrifuge concentrator. Concentrated elutions were injected into a Superdex 200 10/300 GL column. Samples were eluted into a buffer containing 20 mM Tris, 250 mM NaCl, 1% Glycerol, 1 mM dithiothreitol (DTT) and 0.1 mM DDM. pH was set to 8 after mixing all components. Data was collected in .csv format and plotted using R script.

Chapter 3 Results

The human Nup214 β-propeller (hNup214β) and human Nup88 β-propeller (hNup88β) constructs were available in the lab. An agarose gel was run to verify that the plasmids were intact.

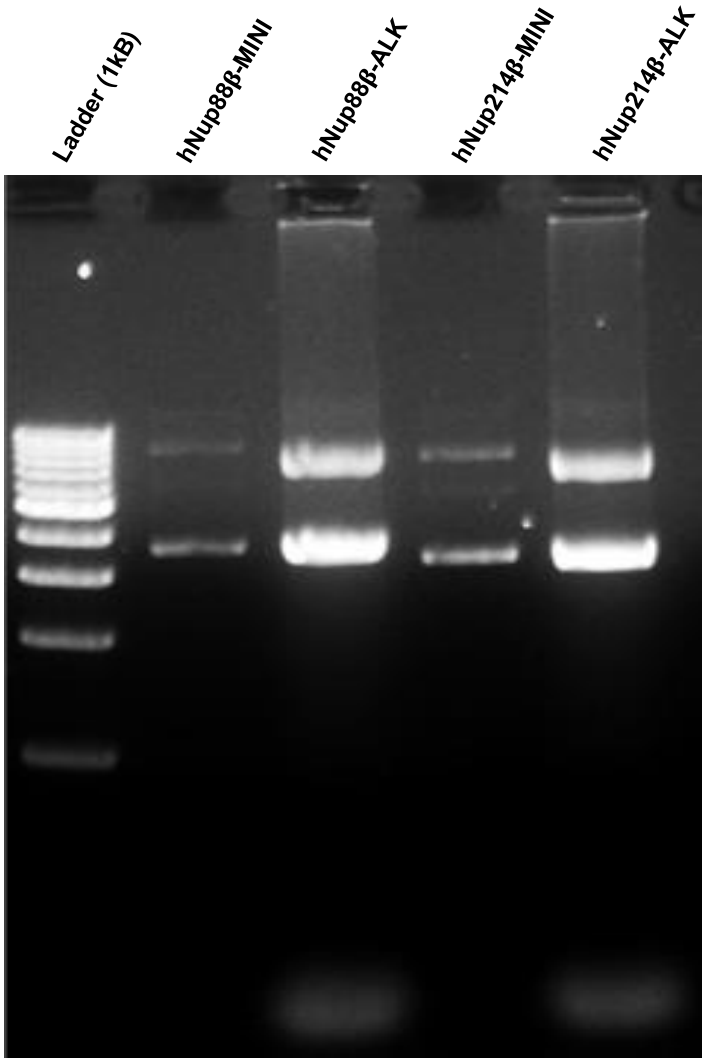

Figure3 0.8% agarose gel run to verify the integrity of the plasmids to be used for purification of hNup214β and hNup88β. hNup88β is in a pET28a vector, with a N-terminal 6xHis tag, while hNup214β is in a pGEX4T1 vector, and has a N-terminal GST tag. Plasmids were isolated from *E. coli* DH5α cells using Mini prep kit or alkaline lysis. Lane 1- Ladder (1kB), Lane 2- hNup88β (Mini isolated), Lane 3- hNup88β (Alkaline lysis isolated), Lane 4- hNup214β (Mini isolated), Lane 5- hNup214β (Alkaline lysis isolated)

Since the plasmids were verified to be intact, optimizing the protocol for purification of the proteins was carried out. A protocol for purification of the rat constructs of the two proteins was used as a starting point and modified accordingly to suit the human constructs. The first step was determining the optimal post-induction time. Two cultures of 1L volume each were induced using 0.45mM IPTG for two different time-points: 4hrs and 9hrs at 18°C respectively. Following that, cells were harvested and lysed by resuspension in lysis buffer 1. The lysate was sonicated on ice at an amplitude of 35 Hz for 18 cycles, with each cycle lasting 10s, and 20s gap between each cycle to prevent overheating. The lysate was then centrifuged at 17,000 rpm for 1 hour at 4°C. The supernatant was then allowed to bind to GST-beads on an end-to-end rotor for 3hrs as the construct has an N-terminal GST-tag. The beads were subjected to 40 Cv wash, followed by elution against 10mM reduced glutathione. Samples were collected at each stage and were run on a 10% SDS-PAGE gel.

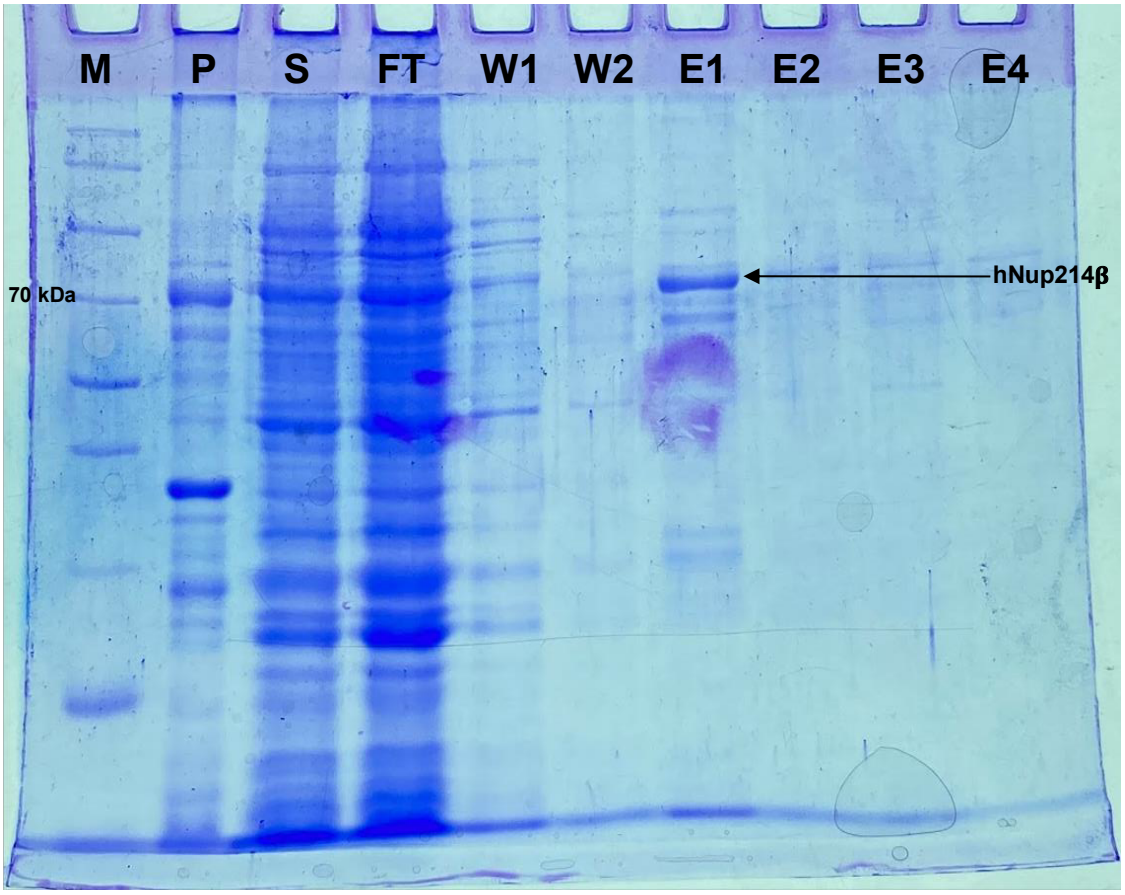

Figure4. hNup214β purification 4hrs post-induction time. Samples collected were run on a 10% SDS-PAGE gel. A thick band in the pellet showed loss of protein in inclusion bodies. Thin bands in the elution lanes showed that concentration of

protein is quite low, due to less production of protein. Lane 1- Marker, Lane 2- Pellet, Lane 3- Supernatant, Lane 4- Flowthrough, Lane 5- Wash 1, Lane 6- Wash 2, Lane 7- Elution 1, Lane 8- Elution 2, Lane 9- Elution 3, Lane 10- Elution 4.

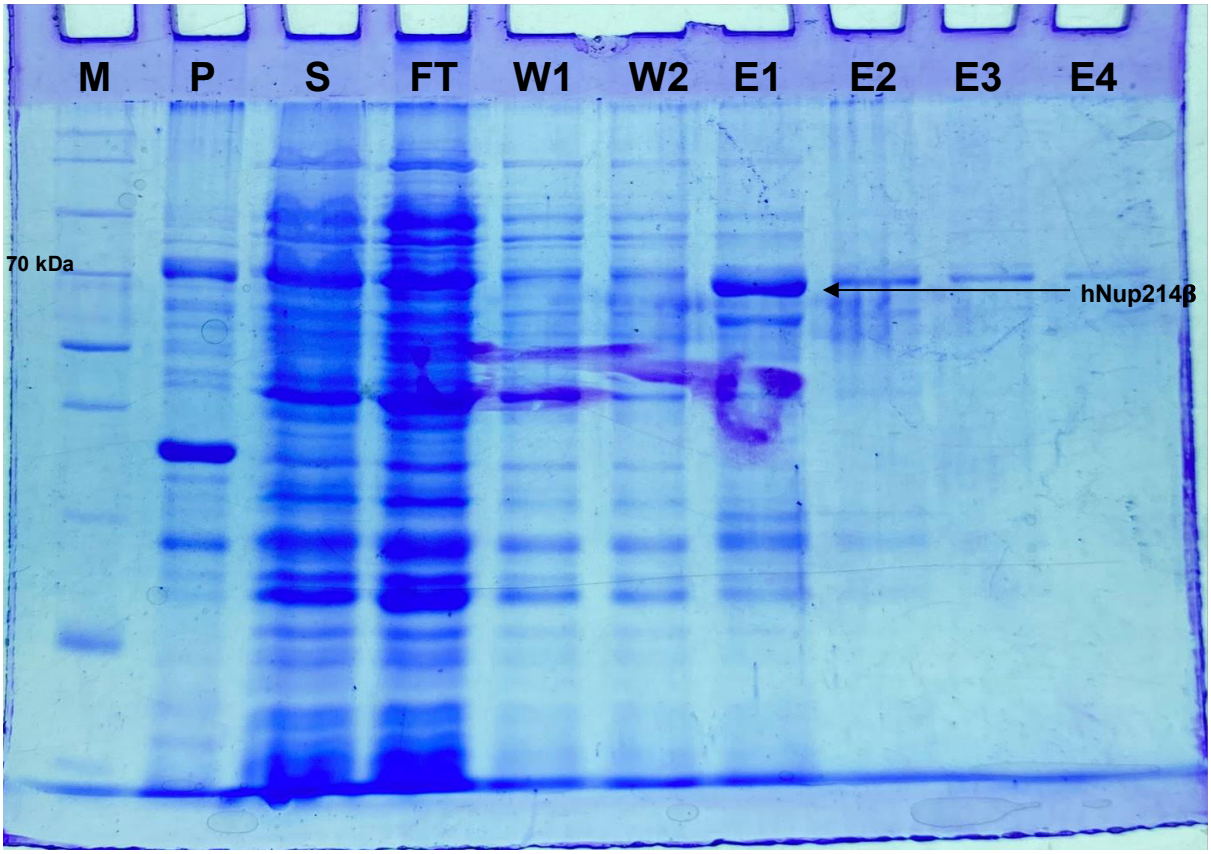

Figure5. hNup214β purification 9hrs post-induction time. Samples collected were run on a 10% SDS-PAGE gel. A thick band in the pellet showed loss of protein in inclusion bodies. In the elutions, while the concentration of protein did increase, the presence of various bands below the expected band lead to the conclusion that there was degradation of protein occurring. Lane 1- Marker, Lane 2- Pellet, Lane 3- Supernatant, Lane 4- Flowthrough, Lane 5- Wash 1, Lane 6- Wash 2, Lane 7- Elution 1, Lane 8- Elution 2, Lane 9- Elution 3, Lane 10- Elution 4.

Based on the above gels, the post-induction time was fixed at 6hrs. To verify that the above protocol would also work for hNup88β, a 2L culture of the construct was harvested and lysed using lysis buffer 2. The same steps were carried out for sonication as well as centrifugation, following which the supernatant was allowed to bind to Ni-NTA beads on an end-to-end rotor for 1hr as the construct has a 6xHis tag at the N-terminus. After bead binding, the beads were washed with 40 Cv wash buffer. Elution 1 was carried out against 100mM imidazole, while the rest of the elutions were carried out against 300mM imidazole. Samples were collected at each stage and were run on a 10% SDS-PAGE gel.

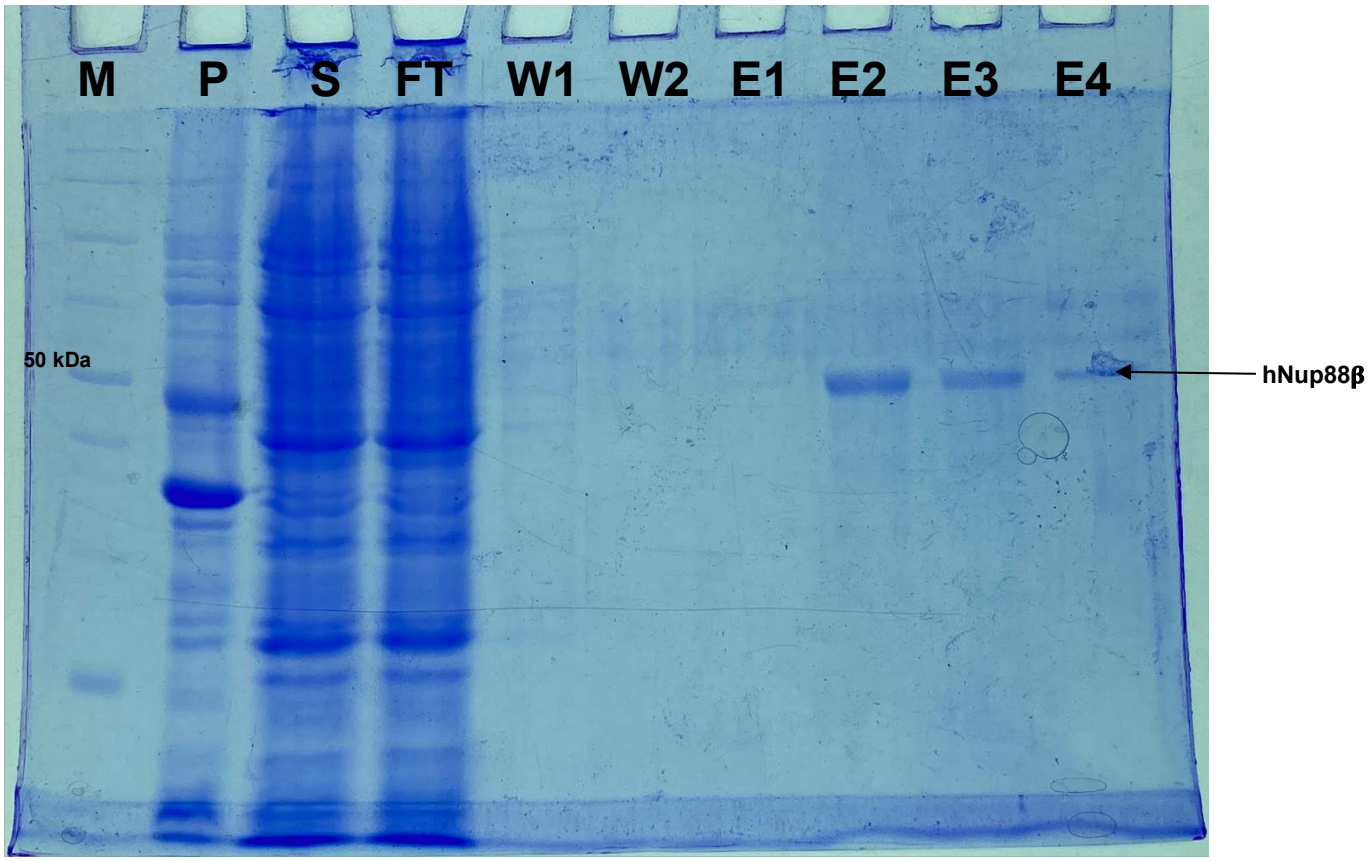

Figure6. hNup88β purification 6hrs post-induction time (Ni-NTA). Samples collected were run on a 10% SDS-PAGE gel. A thick band in the pellet showed loss of protein in inclusion bodies. Elution 1 was carried out against 100mM imidazole, the remaining were carried out against 300mM imidazole. Protocol followed for hNup214β seems to be working fine for hNup88β. Lane 1- Marker, Lane 2- Pellet, Lane 3- Supernatant, Lane 4- Flowthrough, Lane 5- Wash 1, Lane 6- Wash 2, Lane 7- Elution 1, Lane 8- Elution 2, Lane 9- Elution 3, Lane 10- Elution 4.

To ensure reproducibility, 2L cultures of both hNup214β and hNup88β were purified with the buffers mentioned in the table below, and samples run on a 10% SDS-PAGE gel to confirm purification of both proteins.

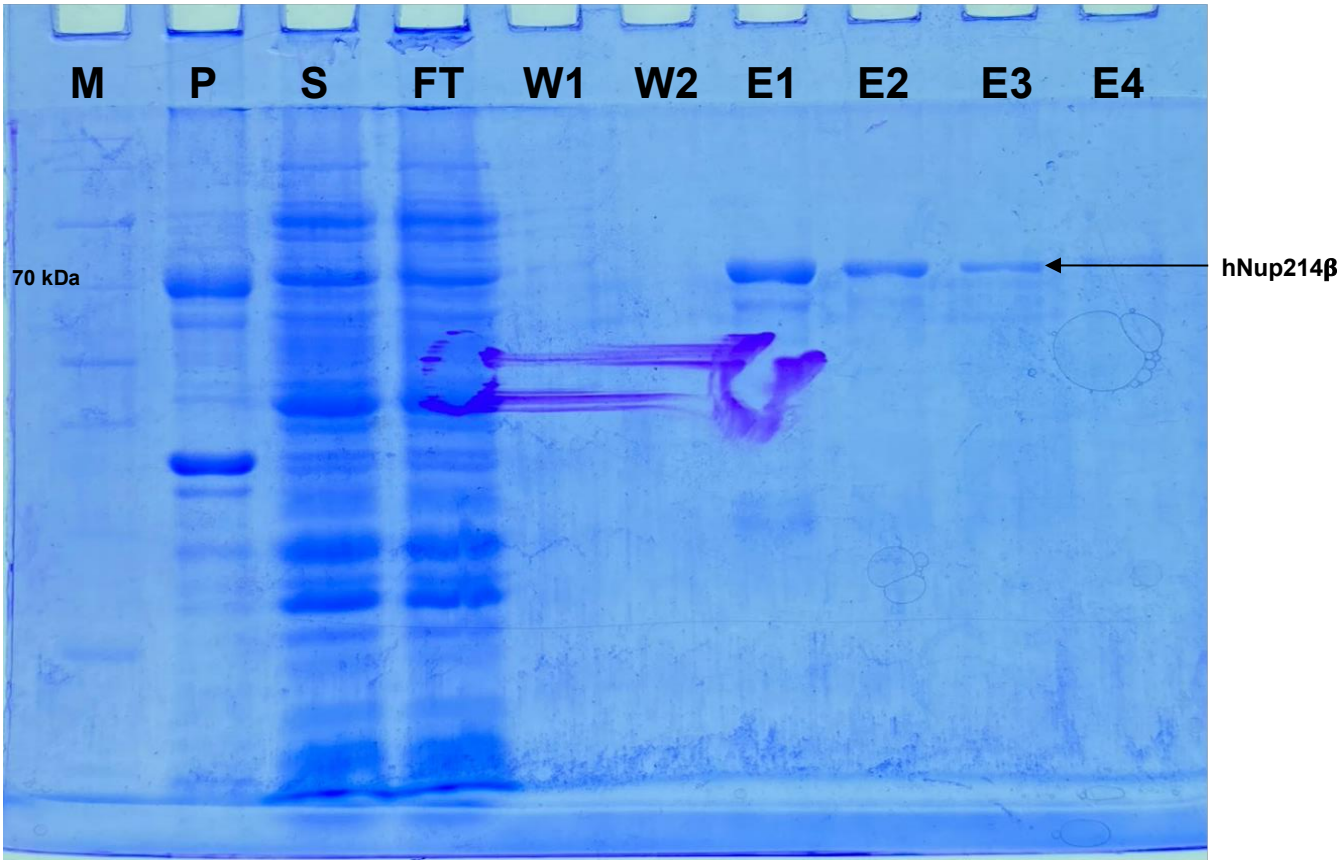

Figure7. hNup214β purification 6hrs post-induction time (GST). Samples collected were run on a 10% SDS-PAGE gel. Elutions were carried out against 10mM reduced glutathione. Protocol observed to be working well for purification. Lane 1- Marker, Lane 2- Pellet, Lane 3- Supernatant, Lane 4- Flowthrough, Lane 5- Wash 1, Lane 6- Wash 2, Lane 7- Elution 1, Lane 8- Elution 2, Lane 9- Elution 3, Lane 10- Elution 4.

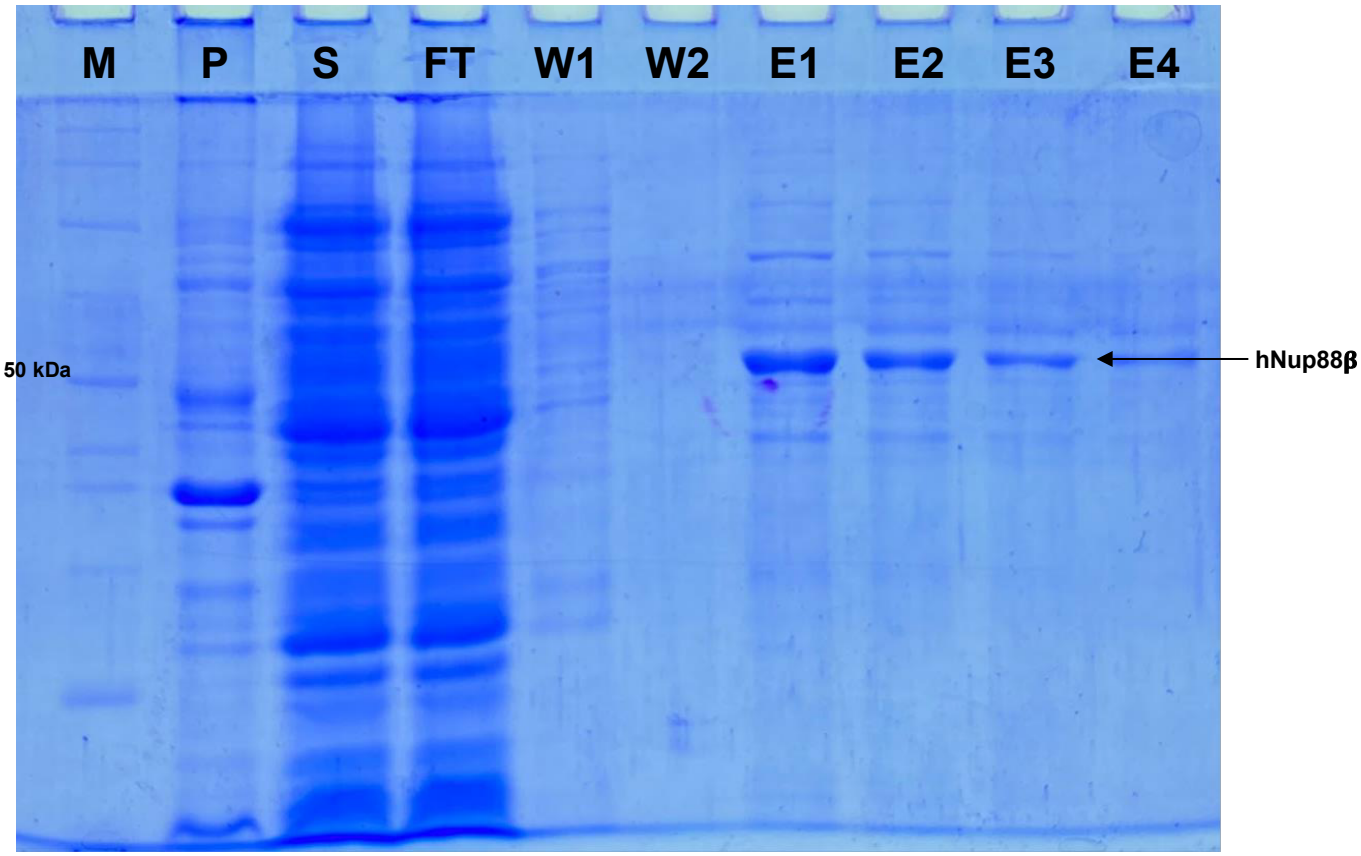

Figure8. hNup88β purification 6hrs post-induction time (Ni-NTA). Samples collected were run on a 10% SDS-PAGE gel. Elutions were carried out against 300mM imidazole. Protocol observed to be working fine for hNup88β purification. Lane 1- Marker, Lane 2- Pellet, Lane 3- Supernatant, Lane 4- Flowthrough, Lane 5- Wash 1, Lane 6- Wash 2, Lane 7- Elution 1, Lane 8- Elution 2, Lane 9- Elution 3, Lane 10- Elution 4.

Following successful purifications of both proteins individually, purification of the hNup214β-hNup88β complex was attempted. Cells were co-transformed with both plasmids, then a 2L culture of co-transformed cells was induced for 6hrs at 18°C using 0.45mM IPTG. The culture was harvested and the proteins purified using Ni-NTA beads. Elution 1 was carried out against 100mM imidazole, while the remaining elutions were carried out against 300mM imidazole. The samples were run on a 10% SDS-PAGE gel. The elution of both proteins was confirmed via Western Blotting.

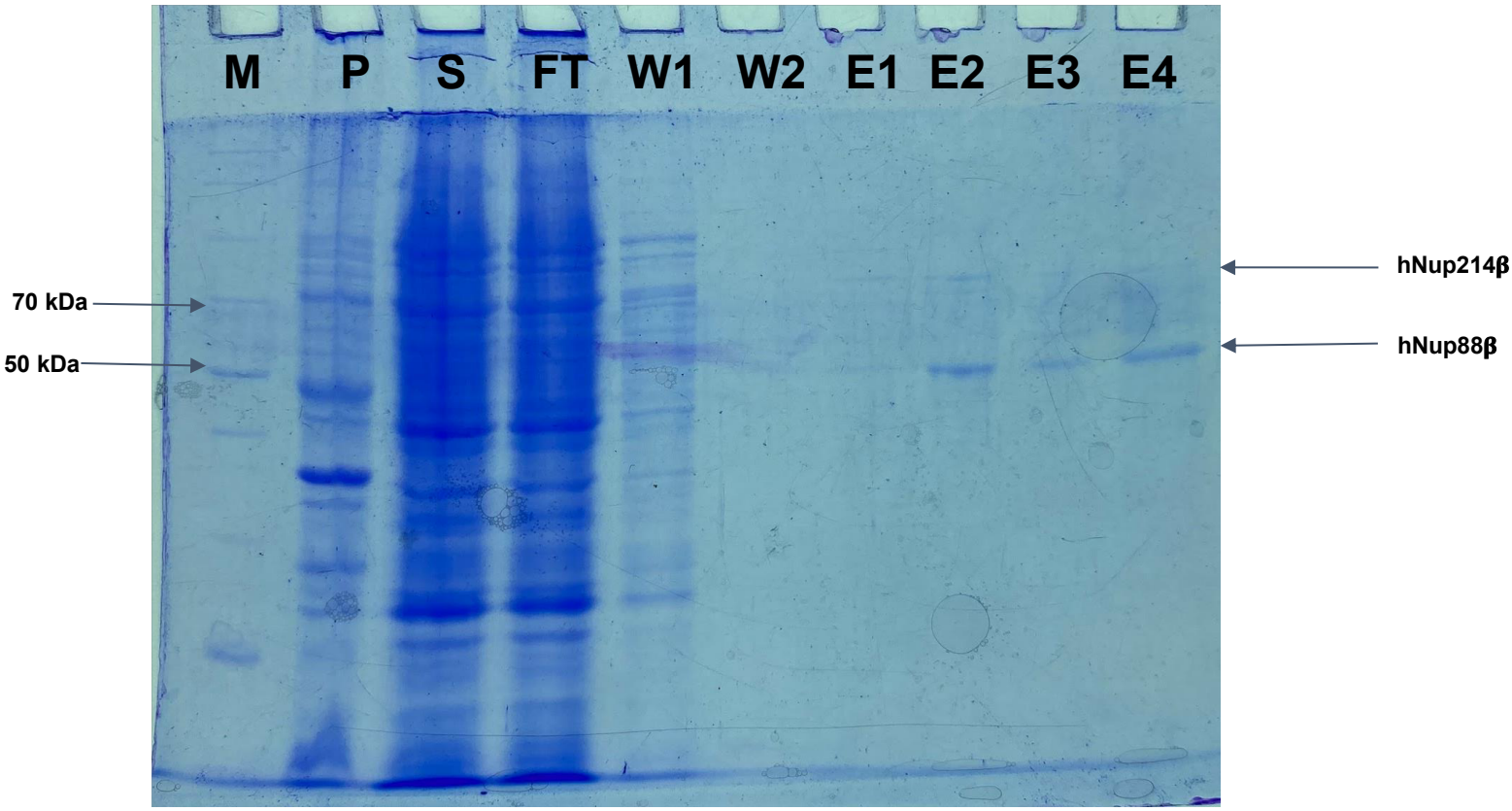

Figure9. hNup214β-hNup88β purification 6hrs post-induction time (Ni-NTA). Samples collected were run on a 10% SDS-PAGE gel. Elution 1 was carried out against 100mM imidazole while remaining elutions were carried out against 300mM imidazole. Protocol observed to be working fine for hNup214β-hNup88β purification. Lane 1- Marker, Lane 2- Pellet, Lane 3- Supernatant, Lane 4- Flowthrough, Lane 5- Wash 1, Lane 6- Wash 2, Lane 7- Elution 1, Lane 8- Elution 2, Lane 9- Elution 3, Lane 10- Elution 4.

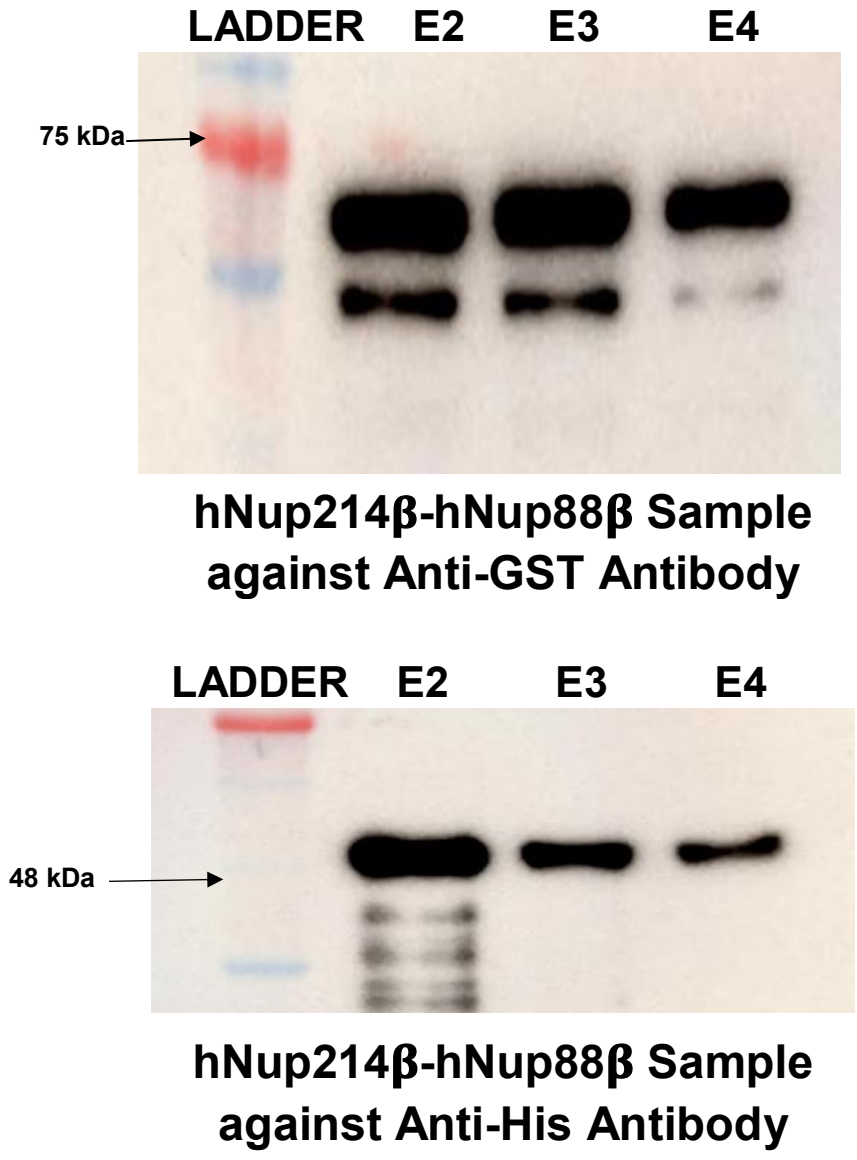

Figure10. Western Blot of hNup214β-hNup88β purification 6hrs post-induction time (Ni-NTA). Anti-GST antibody shows presence of GST tagged hNup214β in the elutions, while Anti-His antibody shows presence of His tagged hNup88β in the elutions.

The purification of the complex was then attempted using GST pulldown. While hNup214β was observed in the eluants, hNup88β was not, which was confirmed by Western Blotting. As a consequence of this, a control experiment was conducted, where the GST tagged hNup214β was bound against Ni-NTA beads. It was observed that hNup214β non-specifically bound to Ni-NTA beads, which was confirmed via Western Blotting.

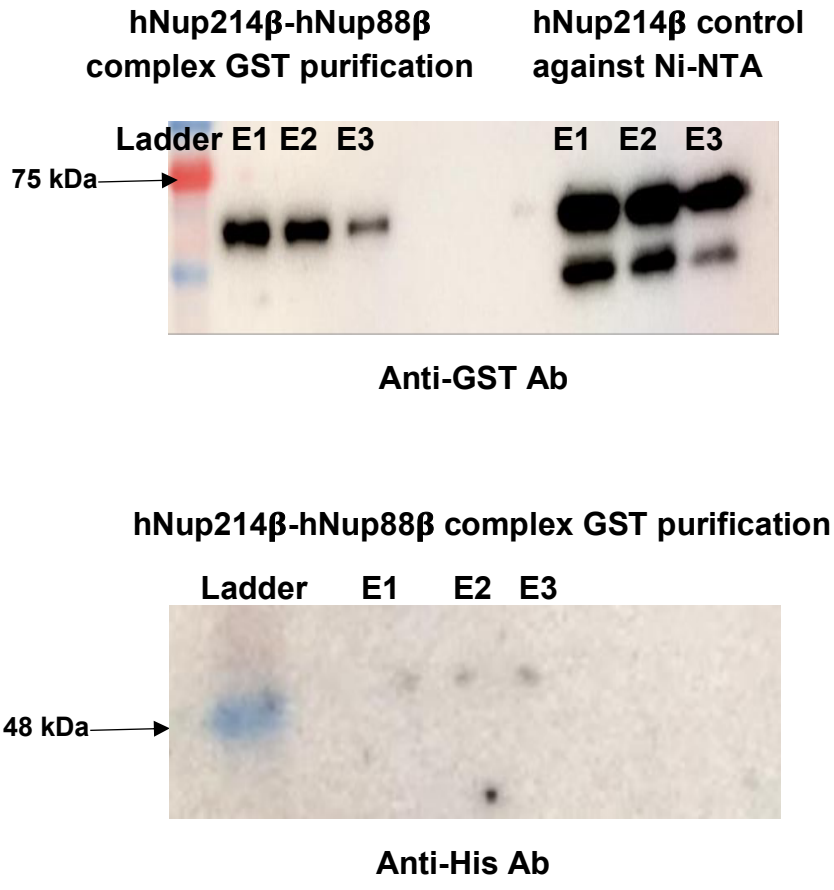

Figure11. Western Blot of hNup214β-hNup88β purification 6hrs post-induction time (GST). Anti-GST antibody shows presence of GST tagged hNup214β in the elutions, while Anti-His antibody does not show presence of His tagged hNup88β in the elutions. Furthermore, elutions show presence of GST tagged hNup214β in a Ni-NTA pulldown, which implies that hNup214β non-specifically binds to Ni-NTA beads.

The observation of the non-specific binding of hNup214β to Ni-NTA beads prompted a deeper look into the sequence and secondary structure of the protein. hNup214β contains 7 histidine residues across its 410 amino acid sequence, however, in its sequence these residues were not observed to be bunched together. Histidine is a negatively charged amino acid residue that is known to bind to Ni-NTA beads. Analysis of the secondary structure showed that 4 histidine residues, in pairs of 2 (a.a. 96,97 and a.a. 303,304), appeared to form a pocket of negative charge that could be the reason for non-specific binding to Ni-NTA beads.

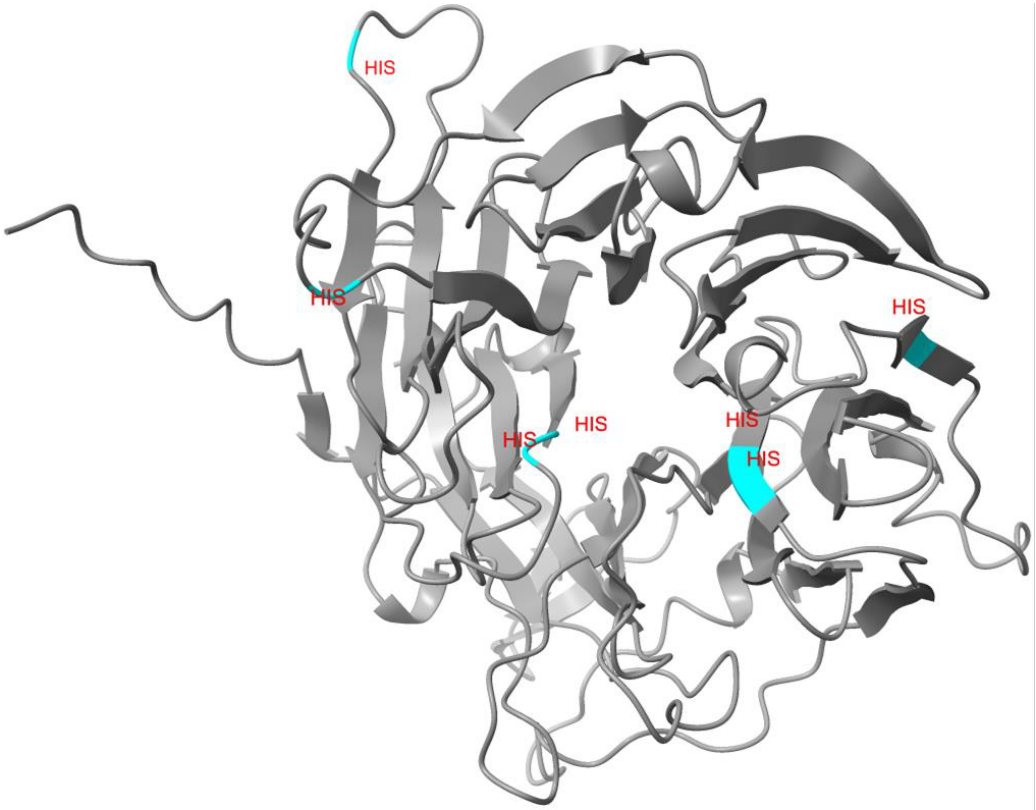

Figure12. Secondary Structure of hNup214β with Histidines marked. The secondary structure of hNup214β is coloured grey, with the 7 histidines labelled in cyan. The two pairs of two histidines together, found at residues 96,97 and 303,304, are suspected to form a pocket of negative charge, which may be a metal ion binding pocket, which could be the reason for non-specific binding to Ni-NTA beads.

Following the above results, tandem purification of the above complex was attempted. A 2L culture of co-transformed cells were induced using 0.45mM IPTG for 16°hrs at 18C. The increased time post induction was to ensure that both cells were given adequate time to produce both proteins. The proteins were first pulled down using Ni-NTA beads, as both proteins were shown to bind to these beads. Following this, the eluants were dialysed overnight in a 10 kDa dialysis bag to remove imidazole from the eluants. The eluants, post dialysis, were then allowed to bind with GST beads on an end-to-end rotor for 3hrs, following which the beads were washed with 40 Cv wash buffer, and eluted against 10mM reduced glutathione. Samples were run on a 10% SDS-PAGE gel. The elutions, however, started precipitating upon concentration, which prevented further studies using this method of purification of the complex.

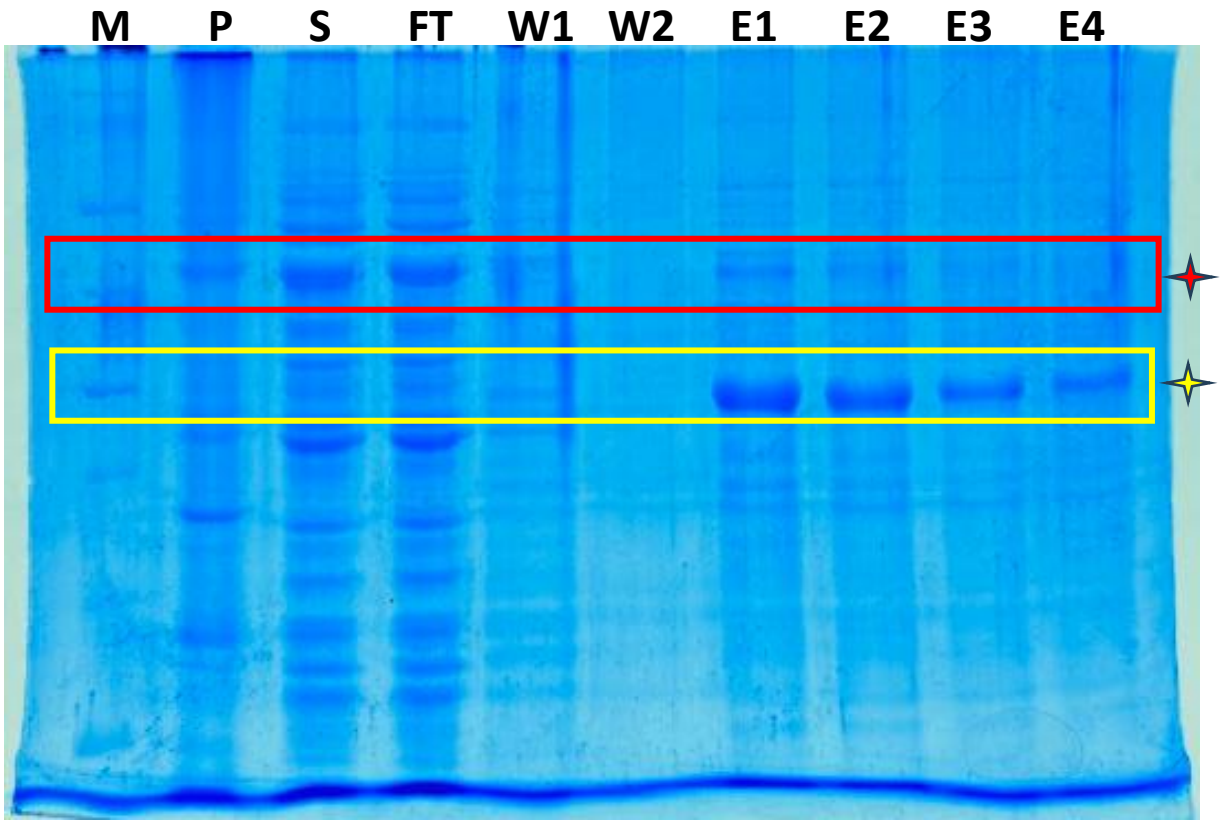

70kDa band – GST hNup214β

50kDa band – 6xHis hNup88β

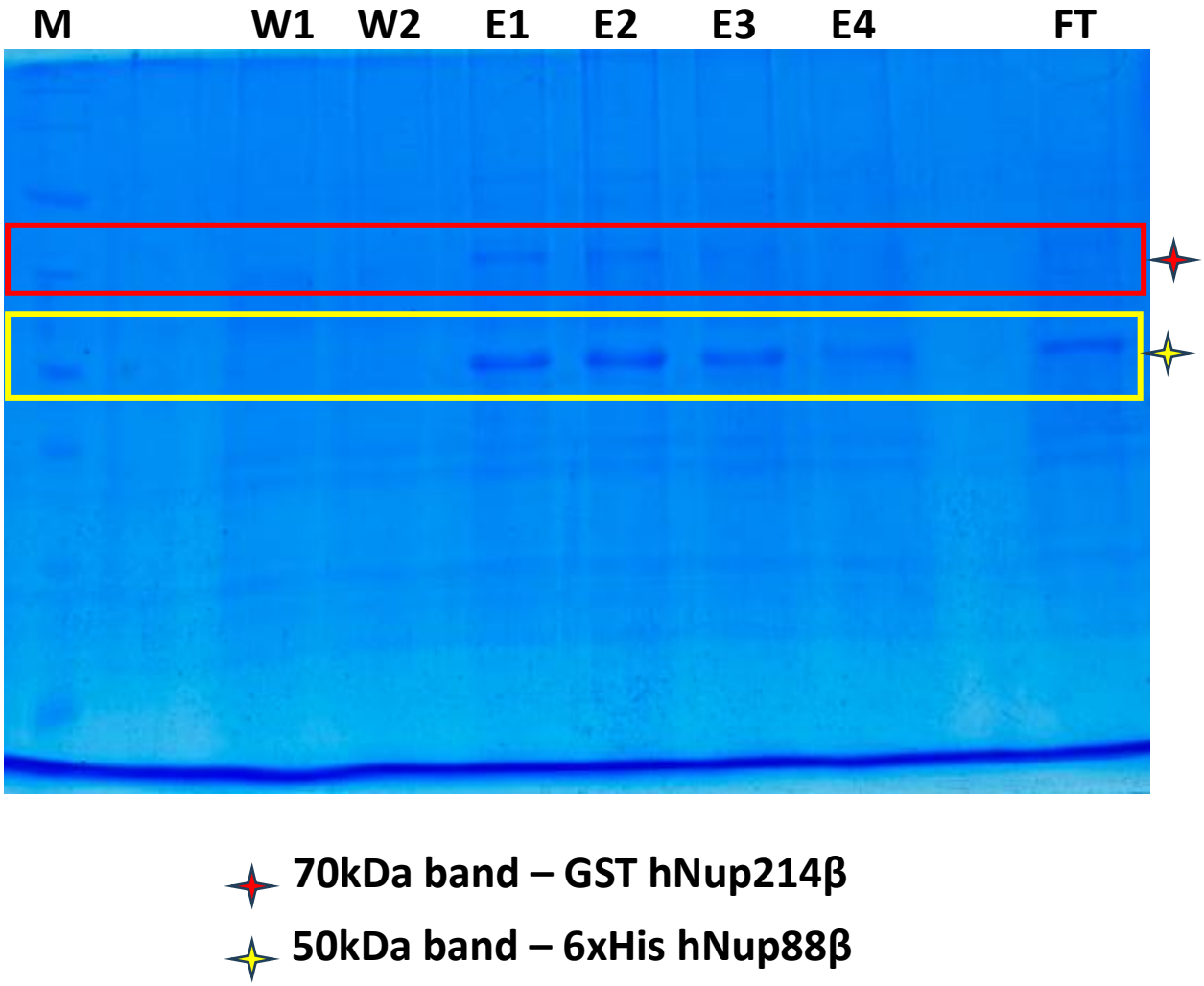

Figure13. Tandem purification (Ni-NTA then GST) ofhNup214β-hNup88β 16hrs post-induction time. Samples collected were run on a 10% SDS-PAGE gel. Ni-NTA purification was carried out first. Elutions were carried out against 300mM imidazole. Eluants were dialysed overnight in a 10 kDa dialysis bag to remove imidazole. Post dialysis, eluants were bound to GST beads, and eluted against 10mM reduced glutathione. Lane 1- Marker, Lane 2- Pellet, Lane 3- Supernatant, Lane 4- Flowthrough, Lane 5- Wash 1, Lane 6- Wash 2, Lane 7- Elution 1, Lane 8- Elution 2, Lane 9- Elution 3, Lane 10- Elution 4.

Given that the first steps of purification were observed to work for the individual proteins, the next step was to purify the eluants further using Size Exclusion Chromatography (SEC).

A 4L culture of hNup214β was purified following the previously followed protocol. Samples were run on a 10% SDS-PAGE gel to confirm protein presence in eluants.

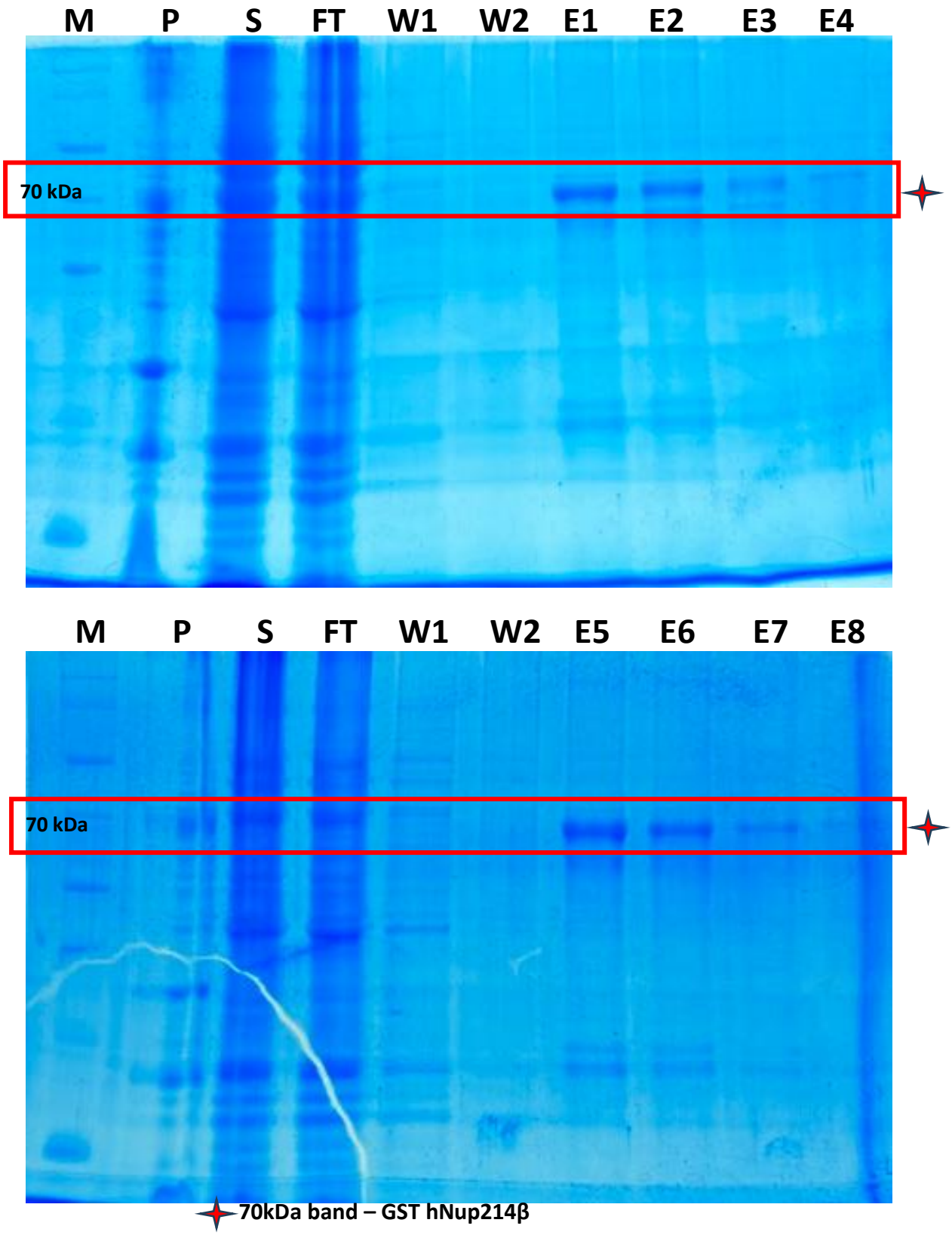

Figure14. hNup214β purification 6hrs post-induction time (GST). Samples collected were run on a 10% SDS-PAGE gel. Elutions were carried out against 10mM reduced glutathione. Protocol observed to be working well for purification. Lane 1- Marker, Lane 2- Pellet, Lane 3- Supernatant, Lane 4- Flowthrough, Lane 5- Wash 1, Lane 6- Wash 2, Lane 7- Elution 1, Lane 8- Elution 2, Lane 9- Elution 3, Lane 10- Elution 4.

Eluants 1 and 2 were concentrated from a volume of 2ml to 0.8ml using a 30 kDa concentrator. The resulting volume was then spun at 15,000 rpm for 10min at 4°C before being injected into a Superdex 200 10/300 column for SEC. The resulting chromatogram was used as reference to pick eluants from the column to run on a 10% SDS-PAGE gel.

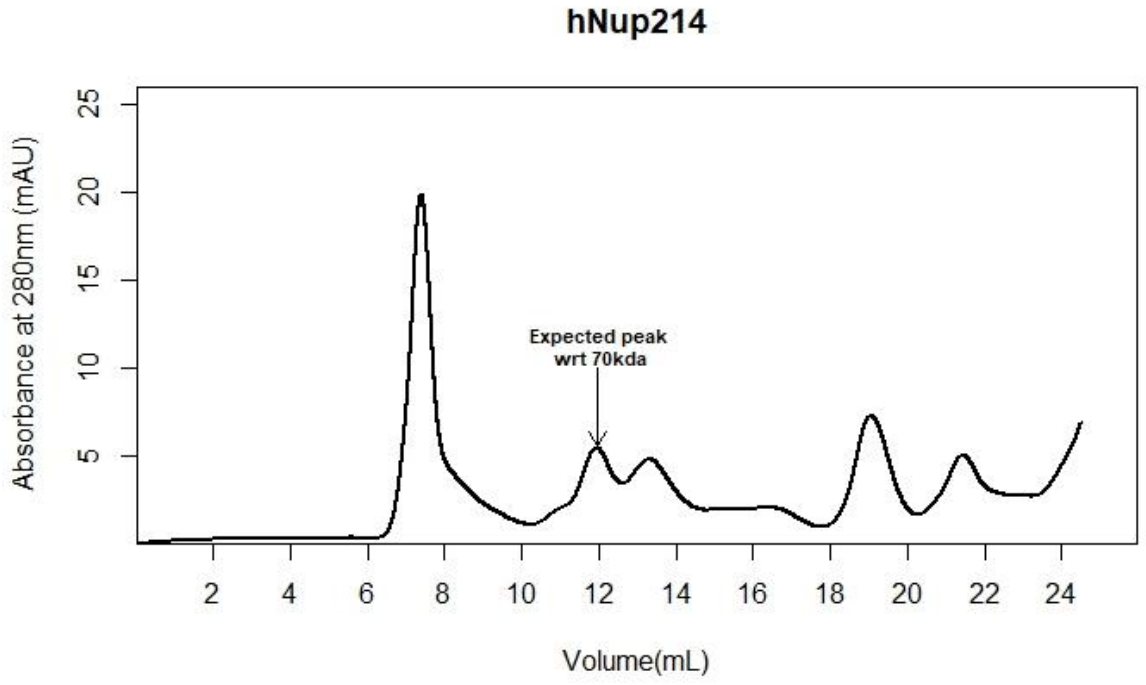

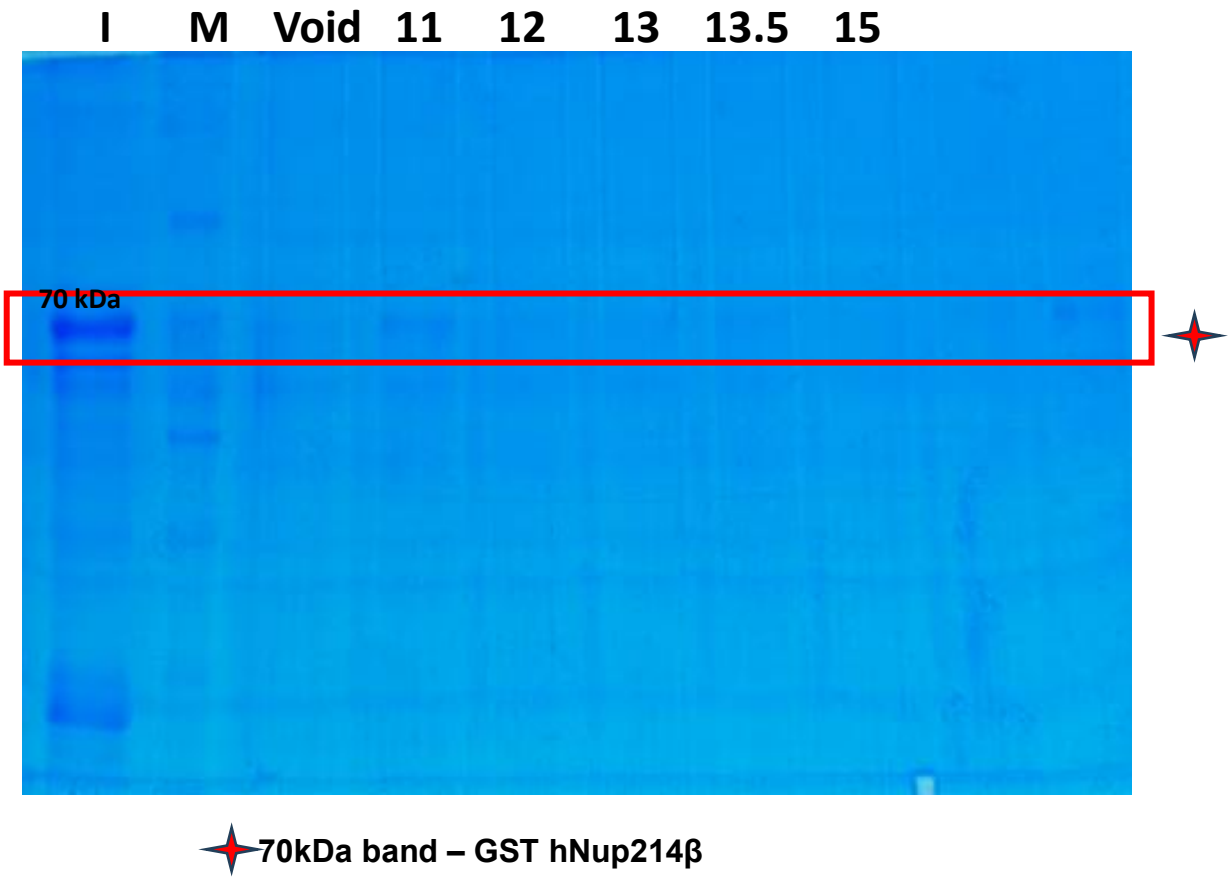

Figure15. Chromatogram and SDS-PAGE gel of GST hNup214β. 500 µL of concentrated sample of E1 and E2 was injected into Superdex 200 10/300 GL column. Chromatogram shows a slight tail of void volume peak which may be indicative of aggregation. Expected peak of GST hNup214β is about 11.5 mL, which is seen, however, there is a twin peak formed without resolving the expected peak. 10% SDS-PAGE gel shows very faint bands of protein, indicative that the protein is highly diluted.

Given the apparent lack of concentration of the protein, as well as the extremely faint bands seen in the SDS-PAGE gel, the remaining 6ml of eluants of the original pulldown were concentrated to 0.8ml and injected into the column. The resulting chromatogram was used as reference to pick eluants from the column to run on a 10% SDS-PAGE gel.

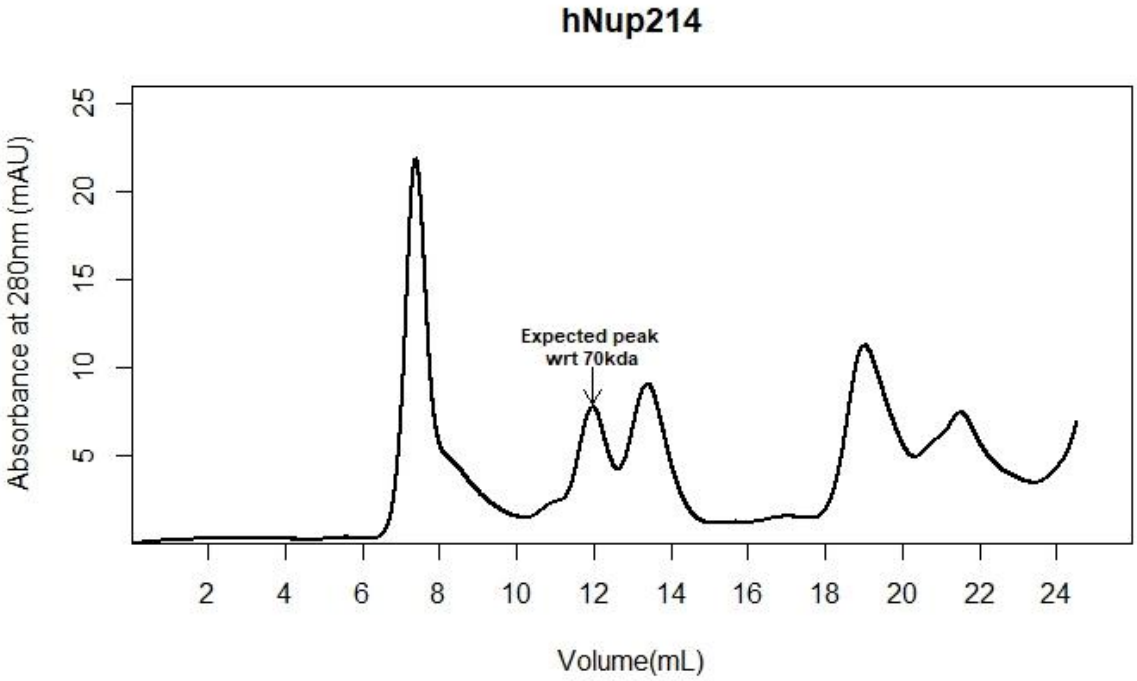

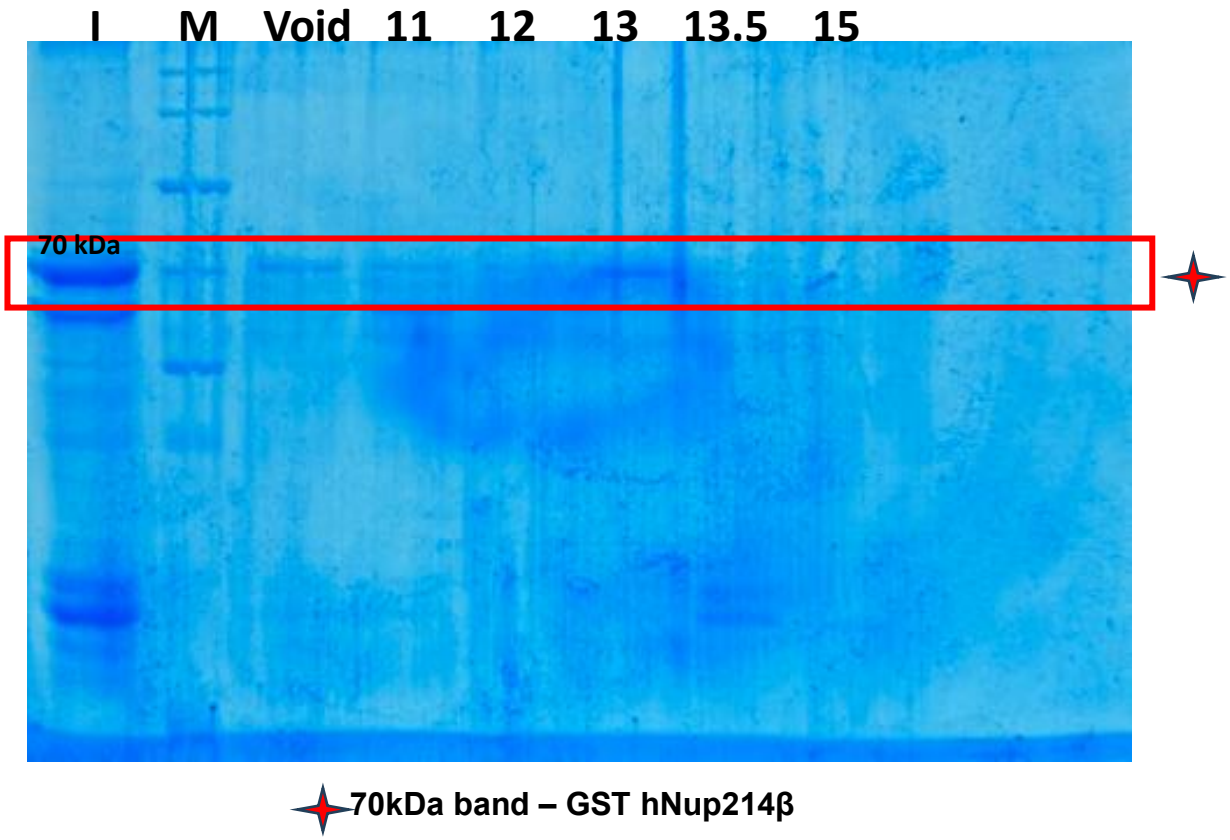

70kDa band – GST hNup214β

Figure16. Chromatogram and SDS-PAGE gel of GST hNup214β. 500 µL of concentrated sample of remaining elutions was injected into Superdex 200 10/300 GL column. Chromatogram shows a slight tail of void volume peak once again, which

may be indicative of aggregation. Expected peak of GST hNup214β is about 11.5 mL, which is seen, however, once again, there is a twin peak formed without resolving the expected peak. 10% SDS-PAGE gel shows faint bands of protein in void volume, which implies that the protein is aggregating. There are also bands below the expected molecular weight of GST hNup214β at 11 ml, which could imply either degradation, or inability to separate contaminants from GST hNup214β.

While both chromatograms showed peaks at the expected volume, a sister peak was observed, which indicated the presence of a contaminant of very close molecular weight, which the column was unable to separate. Furthermore, when samples were spun prior to injection, a large pellet was seen in the tubes. The presence of this large pellet seemed to imply that the protein was aggregating.

As a result, another purification of hNup214β was attempted. To reduce the chances of aggregation, salt concentration was increased to 500mM across all buffers. Elutions were pooled together and concentrated to 0.8 mL. The concentrated protein was spun at 15,000 rpm for 10 minutes at 4°C before being injected into a Suparose 6 column. The resulting chromatogram is shown below.

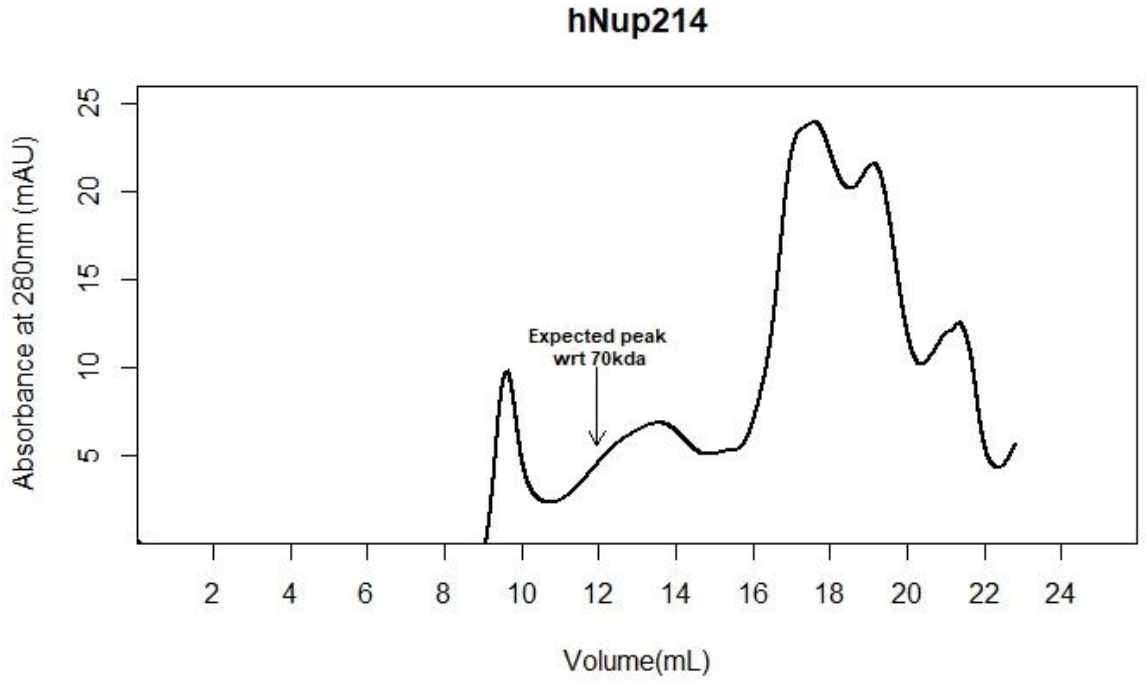

Figure17. Chromatogram of GST hNup214β. 500 µL of concentrated sample was injected into Superose 6 10/300 GL column. Chromatogram shows column unable to resolve any peaks properly, possibly due to precipitation or aggregation of protein that was observed during high spin before injection. 500mM of salt did not help in solubilizing protein better.

All three attempts at performing SEC of hNup214β showed the protein to be aggregating upon concentration.

SEC of hNup88β was then attempted. A 2L culture was induced, then purified with a minor change in the original protocol. In the lysis buffer, 1.5% Triton X-100 was used instead of 1%. When samples were run on a 10% SDS-PAGE gel, it was observed that this increase in detergent concentration reduced the loss of protein in pellet.

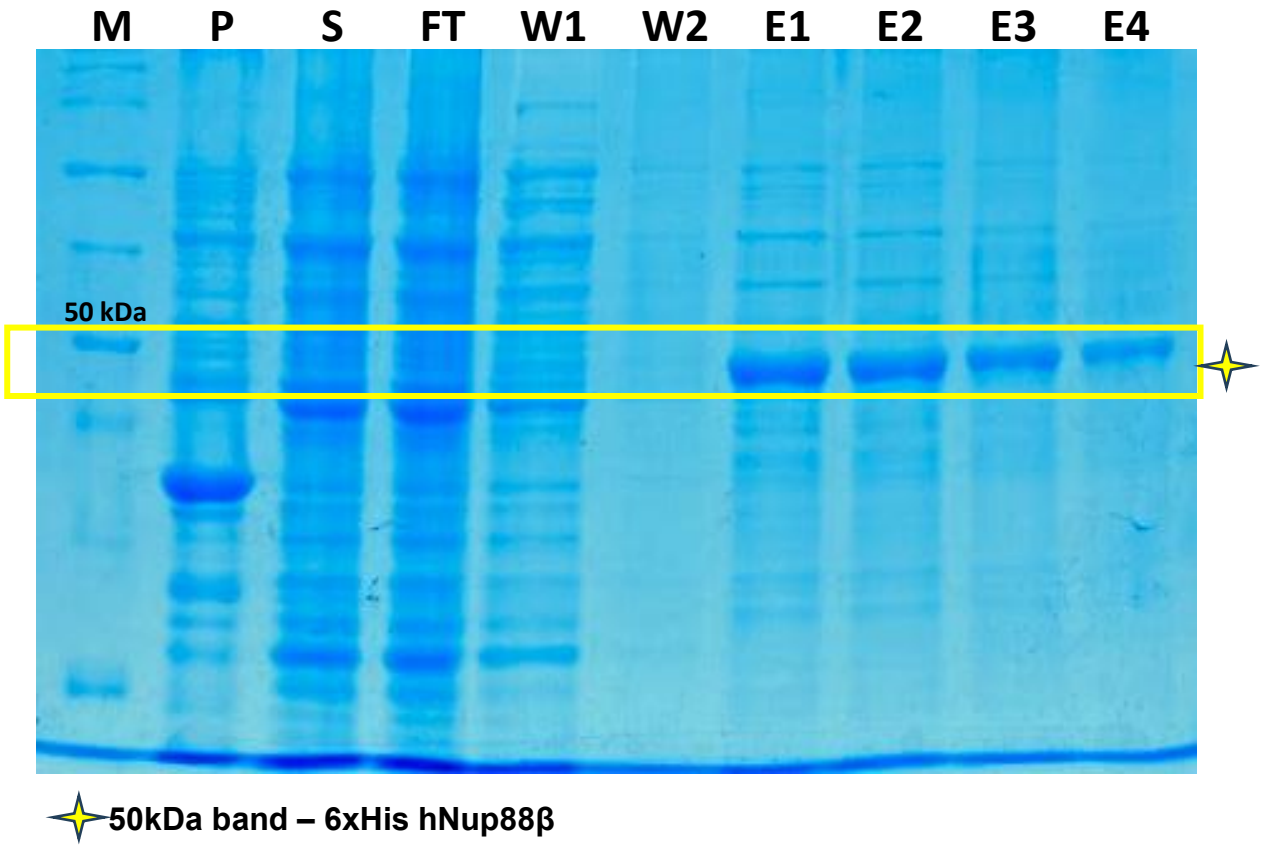

Figure18. hNup88β purification 6hrs post-induction time (Ni-NTA). Samples collected were run on a 10% SDS-PAGE gel. Elutions were carried out against 300mM imidazole. Protocol slightly modified to use 1.5% Triton X-100 in lysis buffer, as a result of which no band of hNup88β seen in pellet. Lane 1- Marker, Lane 2-

Pellet, Lane 3- Supernatant, Lane 4- Flowthrough, Lane 5- Wash 1, Lane 6- Wash 2, Lane 7- Elution 1, Lane 8- Elution 2, Lane 9- Elution 3, Lane 10- Elution 4.

Following confirmation of purification of hNup88β, the eluants were concentrated from 4ml to 2ml using a 30 kDa concentrator. When this sample was spun at 15,000 rpm for 10 minutes at 4°C, a large pellet was observed. When samples of the supernatant and pellet were run on a 10% SDS-PAGE gel, both samples could be seen to contain hNup88β, which lead to the conclusion that this protein too was aggregating upon concentration.

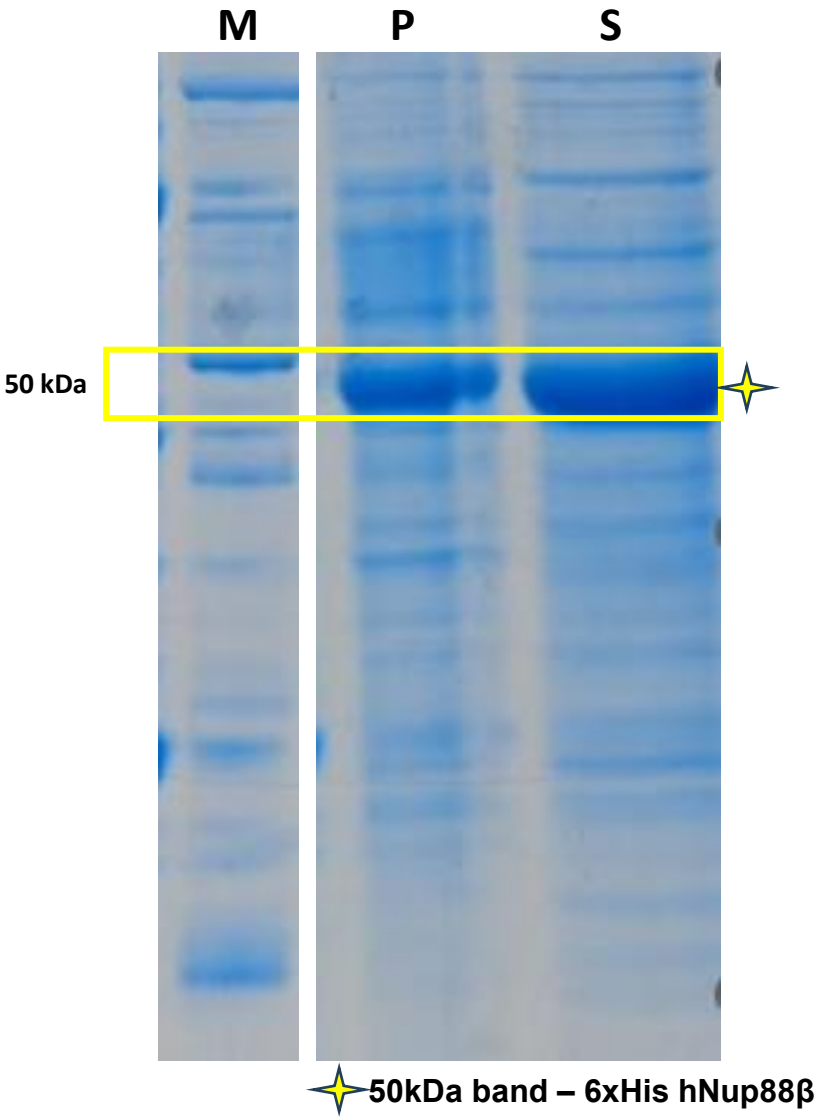

Figure19. Aggregation and precipitation of hNup88β upon concentration. 10% SDS-PAGE gel image of Pellet and supernatant fractions collected after 4mL of elutions concentrated to 2mL and then spun at 15,000 rpm at 4°C. The thick band

that can be seen in the pellet fraction shows that hNup88β is also aggregating and precipitating under concentration, which could be due to poor solubility of the protein.

As a result of this, eluants were not injected into the SEC column, as the protein appears to be insoluble, and prone to aggregation. SEC can cause injected samples to get very dilute and given the poor yield of protein from affinity chromatography so far, injecting into SEC without concentration of eluants was unfeasible.

Along with the purification of hNup214β and hNup88β, *in silico* analysis of these proteins was performed. Given the observation that hNup214β was non-specifically binding to Ni-NTA beads, alongside the histidine pocket that was observed in the secondary structure, it was hypothesized that hNup214β could have a potential to bind to divalent cations. To test this hypothesis, MIB2, a metal ion binding site prediction and docking server was employed to identify the possible metal ion binding sites in the secondary structure of hNup214β. MIB2 can take either the sequence or a structure file as an input, and makes its predictions using either of those inputs. It uses a fragment transformation method, by comparing the protein structure to a database of known metal ion binding residue templates. This is then analysed by a scoring function, which assigns scores to each of the residue templates, based on the probability of a metal ion coming within 3.5 Å of the residue template. The tool was used to identify potential sites for Ni^{2+} as well as Zn^{2+} ions to bind to hNup214β. The top ten scoring predictions for Ni^{2+} and Zn^{2+} respectively are shown in the below tables.

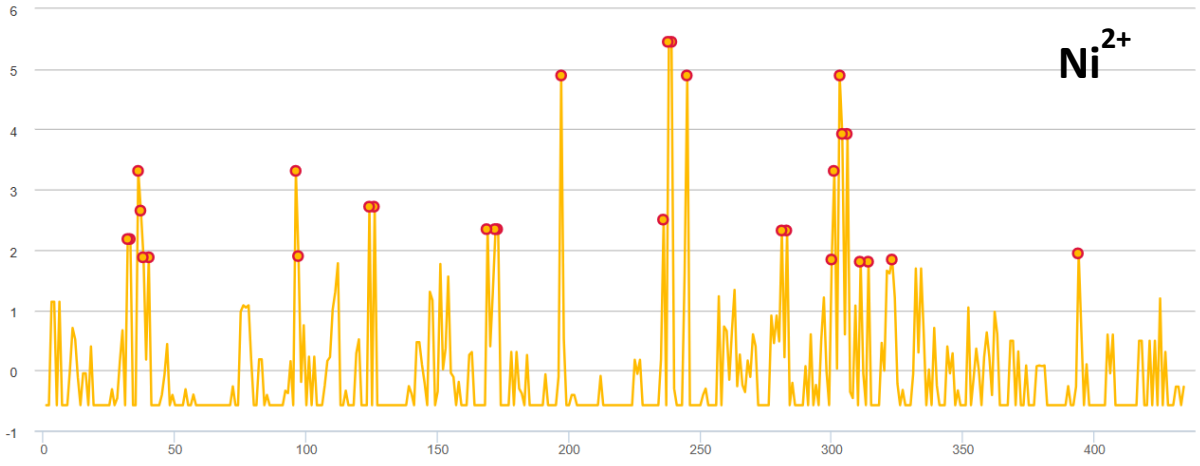

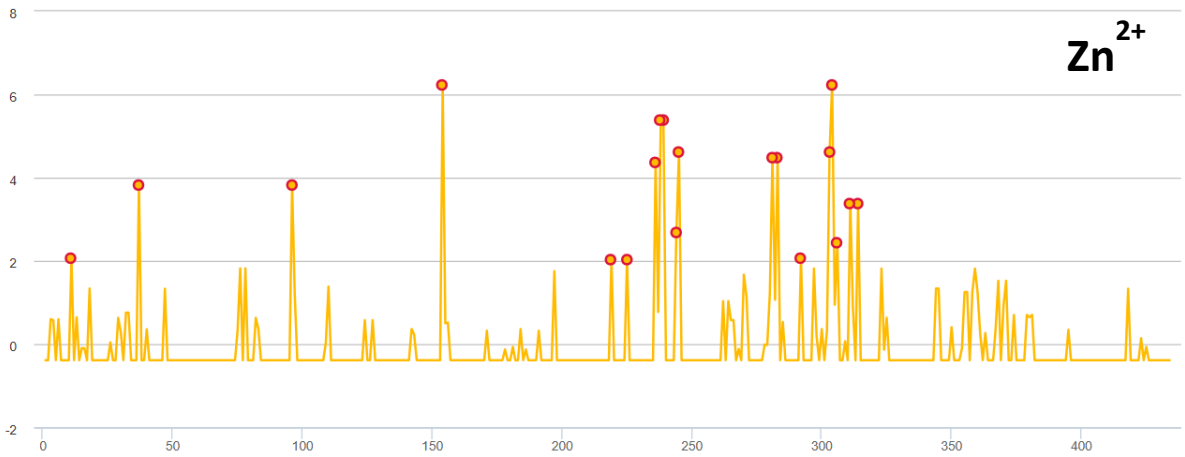

Figure20. Metal ion binding site predictions from MIB2 for Ni^{2+} and Zn^{2+}. The graphs plot the score of each residue of hNup214β. The red open circles represent residues that have a high score and are hence predicted to interact with metal ions.

No.	Residues Predicted	Score
1.	238D, 239H	5.451
2.	197S, 245D, 303H	4.893
3.	304H, 306Y	3.924
4.	36K, 96H, 301R, 304H	3.310
5.	238D, 239H	2.844
6.	304H, 306Y	2.761
7.	124D, 126R	2.716
8.	37E, 96H	2.651
9.	236E, 238D, 239H	2.501
10.	169L, 172G, 173S	2.343

Table 5 Top ten scoring predictions for Ni^{2+} binding.

No.	Residues Predicted	Score
1.	154D, 304H	6.228
2.	238D, 239H	5.384
3.	245D, 303H, 304H	4.616
4.	238D, 239H	4.531
5.	281E, 283H	4.481
6.	236E, 238D, 239H	4.366
7.	238D, 239H	4.045
8.	245D, 304H	4.004
9.	37E, 96H	3.822
10.	238D, 239H	3.767

Table 6 Top ten scoring predictions for Zn^{2+} binding.

No.	Residues Predicted	Score
1.	238D, 239H	5.451
2.	197S, 245D, 303H	4.893
3.	304H, 306Y	3.924
4.	36K, 96H, 301R, 304H	3.310
5.	238D, 239H	2.844
6.	304H, 306Y	2.761
7.	124D, 126R	2.716
8.	37E, 96H	2.651
9.	236E, 238D, 239H	2.501
10.	169L, 172G, 173S	2.343

No.	Residues Predicted	Score
1.	154D, 304H	6.228
2.	238D, 239H	5.384
3.	245D, 303H, 304H	4.616
4.	238D, 239H	4.531
5.	281E, 283H	4.481
6.	236E, 238D, 239H	4.366
7.	238D, 239H	4.045
8.	245D, 304H	4.004
9.	37E, 96H	3.822
10.	238D, 239H	3.767

Table 7 and 8. Comparative analysis of top 10 predictions for Ni^{2+} and Zn^{2+} binding. Residues 238D, 239H are the most predicted sites for interaction between the two. Multiple scores for the same residues represent the different orientations in which the metal ions can bind. 37E, 96H are the next overlapping sites for binding.

The overlap of predicted residue pairs for Ni^{2+} as well as Zn^{2+} ions, along with other histidine residues part of the histidine pocket gave credence to the hypothesis that hNup214β has a metal binding pocket and therefore could interact with a variety of metal ions. This was further supported by similar binding scores observed against other ions such as Ca^{2+}, Mg^{2+} and Cu^{2+}.

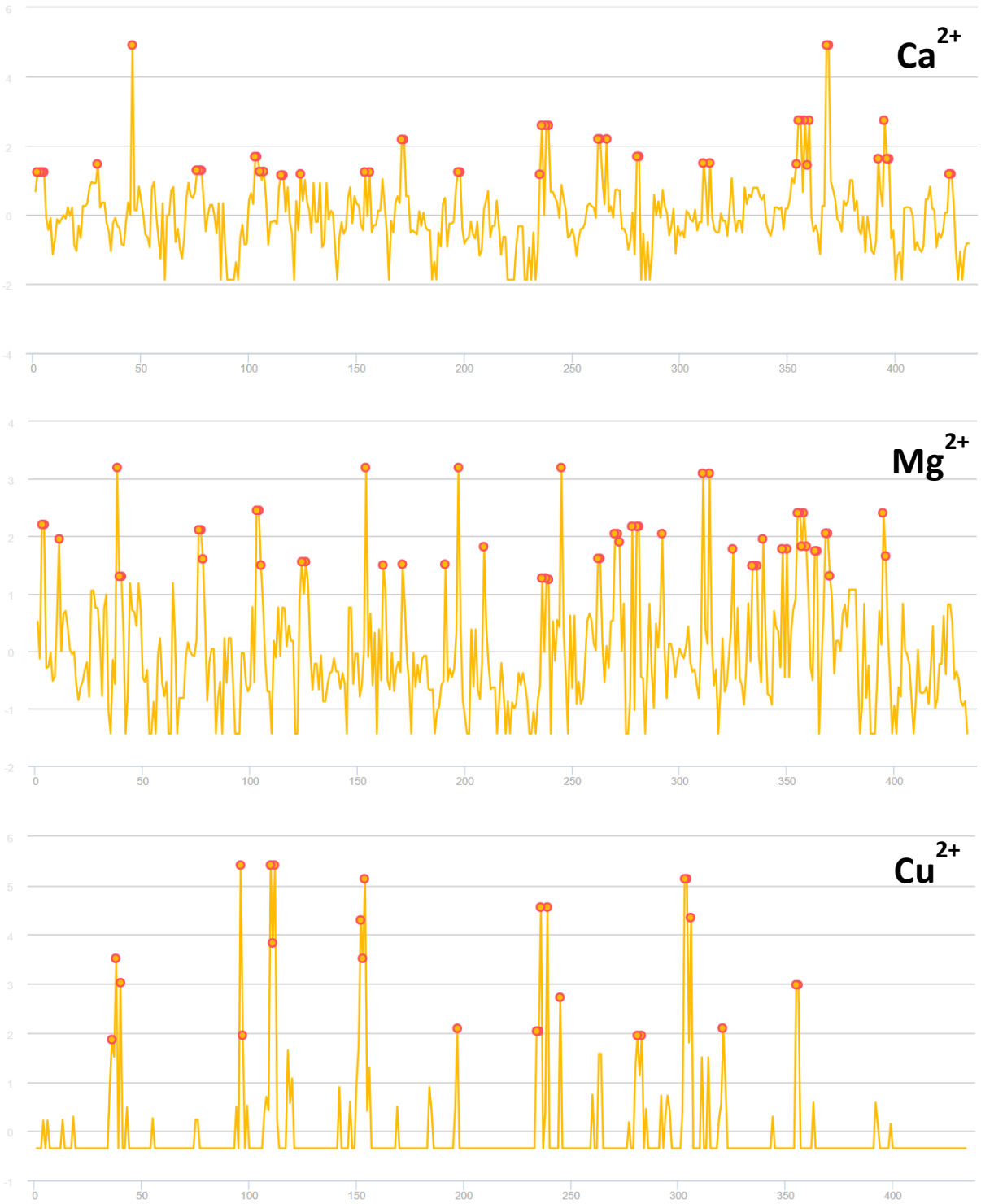

Figure21. Metal ion binding site predictions from MIB2 for Ca^{2+}, Mg^{2+} and Cu^{2+}. The graphs plot the score of each residue of hNup214β. The red open circles represent residues that have a high score and are hence predicted to interact with

metal ions. Residues 96H, 97H, 236E, 238D, 239H, 303H and 304H are predicted to bind to these metal ions as well.

While β-propeller domains are known to have metal ion binding sites in proteins that are not a part of the NPC (RACK1, WDR5 etc.), the presence of metal ion binding sites in β-propeller domains of NPC proteins has not been studied extensively. By virtue of providing conformational stability, as well as potentially helping in protein-protein interactions, as seen in other β-propeller domains, the significance of identifying a potential metal ion binding site warrants greater study.

The β-propeller domains of Nup155 and Nup53 have been shown to bind to membranes previously. To check whether hNup214β and hNup88β might exhibit similar membrane binding propensity, a tool named Protein-Membrane Interaction Predictor (PMIPred^{TM}) was used to identify membrane binding as well as curvature sensing regions within hNup214β and hNup88β. hNup155β (1-515 a.a.) was also run through this tool, to be used as a positive control. Utilizing sequence-based features relevant to membrane-binding (amino acid composition, secondary structure prediction, hydrophobicity, charge and solvent accessibility) and feeding this data to a random forest classifier, the tool was able to predict membrane binding as well as curvature sensing regions in the case of all three input proteins, hNup155β, hNup214β and hNup88β. The predicted regions are shown below.

NAME	hNup155β	hNup88β	hNup214β
CURVATURE SENSING REGIONS (ORANGE)	1. MPSSLLGAAMPASTSAAALQEA(1-21) 2. LSVPN (73-77) 3. NLQTGSGVLNDSL (182-194) 4. EAGWFSQ (243-249) 5. SSL (259-261) 6. TFSE (272-275)	1. ALS (94-96) 2. KRWG (138-141) 3. LFGQNGKDE (253-261) 4. RID (356-358) 5. KFL (426-428)	1. IVDKV (80-84) 2. NEAKQQKRP (130-138) 3. YESD (235-238) 4. KKEEKHP (278-284)
MEMBRANE BINDING REGIONS (MAGENTA)	A. EQFGHMQ (95-101) B. SFLVPSLLQF (262-271)	A. ECLIWPLLSTV (488-498)	No Membrane binding region predicted
STRUCTURE	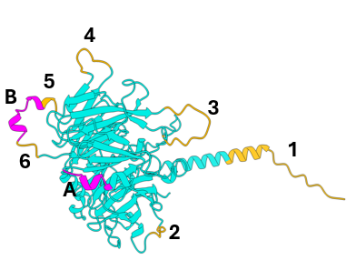	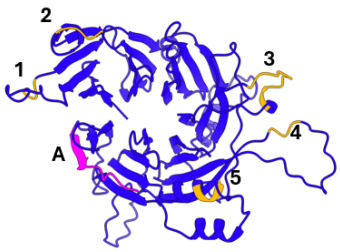	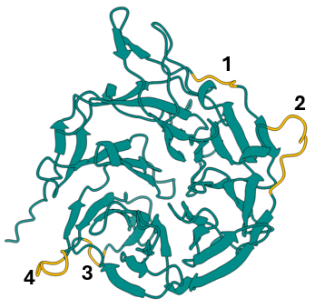

Table 9. Curvature sensing and membrane binding regions of hNup155β, hNup214β and hNup88β by PMIPred^{TM}. The table shows a comparative analysis of

the curvature sensing(orange) and membrane binding(magenta) regions of hNup155β, hNup214β and hNup88β. hNup155β is known to interact with membranes and is used as a positive control. hNup88β is predicted to have 1 membrane binding region and 5 curvature sensing regions, while hNup214β is predicted to have 4 curvature sensing regions, but is not predicted to bind to membranes.

As has been shown previously, hNup155β has a membrane binding loop (258-267 a.a.) (Magistris et al., 2018). The tool has also predicted this loop, which leads credence to the results generated by PMIPred. The presence of membrane binding sites in hNup88β is a previously unreported result, and points towards the possibility that it is involved in providing some level of structural stability to the cytoplasmic filaments of the NPC. Furthermore, lack of a direct membrane binding region in hNup214β also tracks with the belief that this domain is highly involved in facilitating transport across the NPC, and as such requires a degree of flexibility to execute that function. *In vitro* studies such as liposome assays would help in validating these predictions.

Chapter 4 Discussion

The main objective of this study was to gain a deeper understanding of hNup214β and hNup88β. Structural analysis alongside purification of hNup214β showed the presence of a possible metal binding pocket, which was supported by the MIB2 prediction tool. One possible way of confirming this would be to incubate pure protein with metal ions and then perform spectroscopic analysis to check for metal ion binding. The presence of a metal ion binding site in hNup214β can have interesting implications when looking at nucleocytoplasmic transport. hNup214 is known to interact with a wide range of proteins, both during import as well as export across the NPC. Metal ions often bind to proteins that are being transported across the NPC to allow for the transport of these metal ions as well. Nup214 may be involved in transporting these proteins due to them having metal ions bound to them, that can also interact with hNup214β.

In silico analysis of hNup214β and hNup88β along with hNup155β as a positive control using PMIPred™ revealed that hNup214β contains possible curvature sensing regions, while hNup88β contains both curvature sensing as well as membrane binding regions. A possible way to study this would be to perform a liposome pelleting assay with pure protein. Having membrane binding as well as curvature sensing regions points towards the possibility that these domains play a role in the anchoring of the cytoplasmic filament complex of the NPC to the nuclear membrane, and crucially, could be amongst the first Nups of the cytoplasmic filament complex to be recruited during the assembly of new NPCs.

In vitro purification of both hNup214β and hNup88β was attempted. While both proteins were expressing well and were being purified in the first stage via affinity pulldown, concentration of the eluants appeared to be leading to protein aggregation and precipitation. This was further seen when performing SEC of these eluants, where the column was unable to resolve the peaks, and the void volume peak had a large tail that formed a part of the next peak, at the expected volume. These observations point to the possibility that the constructs chosen for purification are insoluble in solution. A possible reason for this insolubility could be that the proteins are unable to fold properly or completely. Given the strict β-propeller domain boundaries taken while

designing these constructs, it is possible that additional amino acid residues could help in allowing the protein to fold properly, as well as allow the protein to solubilize well. The lack of crystal structure of the hNup88β alone further points to the fact that the β-propeller domain of this Nup is not highly soluble *in vitro*. It also is possible that there are some vital post-translational modifications that are required to solubilize the protein, which are not possible when over expressing this construct in a bacterial system.

Chapter 5 References

Hetzer MW. (2010). The nuclear envelope. *Cold Spring Harbor Perspectives in Biology* 2(3): a000539.

Wente SR, Rout MP. (2010). The nuclear pore complex and nuclear transport. *Cold Spring Harbor Perspectives in Biology* 2(10): a000562.

Alber F, Dokudovskaya S, Veenhoff LM, Zhang W, Kipper J, Devos D, Suprapto A, Karni-Schmidt O, Williams R, Chait BT, Sali A, Rout MP. (2007). The molecular architecture of the nuclear pore complex. *Nature* 450(7170): 695–701.

Lin DH, Hoelz A. (2019). The structure of the nuclear pore complex. *Annual Review of Biochemistry* 88: 725–783.

Huang G, Zhang Y, Zhu X, Zeng C, Ran W, Zhao Y, Wang X, Shi Y, He J, Shen Y. (2022). Structure of the inner ring complex of the nuclear pore. *Nature* 609(7926): 603–609.

Stuwe T, Bley CJ, Thierbach K, Petrovic S, Schilbach S, Mayo DJ, Perriches T, Rundlet EJ, Jeon YE, Collins R, Huber FM, Lin DH, Paduch M, Koide A, Koide S, Hoelz A. (2022). Architecture of the cytoplasmic ring of the nuclear pore complex. *Science* 375(6578): eabm9129.

Hutten S, Kehlenbach RH. (2006). Nup214 is required for CRM1-dependent nuclear protein export in vivo. *Molecular and Cellular Biology* 26(18): 6772–6785.

Li Y, Hassinger L, Thomson T, Ding B, Ashley J, Hassinger W, Budnik V. (2021). Nup214 and Nup88 form a complex with Nup62 to regulate mRNA export. *Cell Research* 31(3): 239–256.

Vollmer B, Schooley A, Sachdev R, Eisenhardt N, Schneider AM, Sieverding C, Madlung J, Gerken U, Macek B, Antonin W. (2012). *Direct interaction with Nup153 mediates binding of Tpr to the nuclear pore complex. Molecular Biology of the Cell* 23(5): 973–982.

Antonin W, Ellenberg J, Dultz E. (2008). Nuclear pore complex assembly through the cell cycle: Regulation and membrane organization. *FEBS Letters* 582(14): 2004–2016.

Frey S, Richter RP, Görlich D. (2006). FG-rich repeats of nuclear pore proteins form a three-dimensional meshwork with hydrogel-like properties. *Science* 314(5800): 815–817.

Kelley K, Knockenhauer KE, Kabachinski G, Schwartz TU. (2015). Atomic structure of the Y complex of the nuclear pore. *Nature Structural & Molecular Biology* 22(5): 425–431.

von Appen A, Kosinski J, Sparks L, Ori A, DiGuilio AL, Vollmer B, Mackmull MT, Banterle N, Parca L, Kastritis P, et al. (2015). In situ structural analysis of the human nuclear pore complex. *Nature* 526(7571): 140–143.

Ma J, Goryaynov A, Sarma A, Yang W. (2016). Self-regulated viscous channel in the nuclear pore complex. *Proceedings of the National Academy of Sciences of the United States of America* 113(36): 12493–12498.

Beck M, Fischer JB, Kastritis PL, Schuller JM. (2022). In-cell architecture of the nuclear pore and snapshots of its turnover. *Science* 375(6578): eabm8181.

Bley CJ, Nie S, Mobbs GW, Petrovic S, Gres AT, Liu X, Mukherjee S, Harvey S, Huber FM, Lin DH, Brown B, Hoelz A. (2022). Architecture of the cytoplasmic face of the nuclear pore. *Science* 376(6598): eabm9129.

Napetschnig J, Blobel G, Hoelz A. (2007). Crystal structure of the N-terminal domain of the human protooncogene Nup214/CAN. *Proceedings of the National Academy of Sciences of the United States of America* 104(5): 1783–1788.

Bernad R, Van Overloop H, Trepte P, Schaffner-Reckinger E, Huber ST, Bley N, Stöhr N, Hondele M, Weis K. (2022). The coiled-coil domain of Nup88 mediates its interaction with Nup214, forming a stable heterodimeric complex essential for the structural integrity of the cytoplasmic ring. *Molecular Biology of the Cell* 33(8): ar57.

Port SA, Monecke T, Dickmanns A, Spillner C, Hofele R, Urlaub H, Ficner R, Görlich D. (2015). Structural and functional characterization of CRM1-Nup214 interactions reveals multiple FG-binding sites involved in nuclear export. *Cell Reports* 13(4): 690–702.

Bono F, Cook A, Grünwald M, Ebert J, Conti E. (2010). The crystal structure of the Nup214-Nup88 complex reveals a conserved interface between nucleoporins. *Journal of Biological Chemistry* 285(45): 34911–34918.

Schwartz TU, Modafferi S, Kent HM, Stewart M. (2015). The structure of the Nup214-Nup88 complex reveals a conserved interface in nuclear pore complexes. *Nat Struct Mol Biol.* 22(6):503-507.

Monecke T, Dickmanns A, Urlaub R, Ficner R. 2009. Crystal structure of the N-terminal domain of Nup214 reveals a conserved interface between nucleoporins and exportins. J Biol Chem. 284(35):23540-23548.

Madheshiya PK, Shukla E, Singh J, Bawaria S, Ansari MY, Chauhan R. 2022. Insights into the role of Nup62 and Nup93 in assembling cytoplasmic ring and central transport channel of the nuclear pore complex. *Mol Biol Cell*. 33(4):ar27.

Hutten S, Walde S, Spillner C, Hauber J, Kehlenbach RH. 2016. The nuclear pore component Nup358 promotes transportin-dependent nuclear import. Nat Commun. 7:11482.

Hamed M, Caspar B, Port SA, Kehlenbach RH. 2021. A nuclear export sequence promotes CRM1-dependent targeting of the nucleoporin Nup214 to the nuclear pore complex. J Cell Sci. 134(6):jcs258095.

Gaik M, Flemming D, von Appen A, Kastritis P, Mücke N, Fischer J, Stelter P, Ori A, Bui KH, Baßler J, Barbar E, Beck M, Hurt E. 2015. Structural basis for assembly and function of the Nup82 complex in the nuclear pore scaffold. J Cell Biol. 208(3):283-297.

Vollmer B, Schooley A, Sachdev R, Eisenhardt N, Schneider AM, Sieverding C, Madlung J, Gerken U, Macek B, Antonin W. 2015. A self-inhibitory interaction within Nup155 and membrane binding are required for nuclear pore complex formation. J Cell Sci. 128(7): 1322-1333.

Vollmer B, Antonin W. 2012. Dimerization and direct membrane interaction of Nup53 contribute to nuclear pore complex assembly. EMBO J. 32(4): 316-326.

Chang, Y.-C., Yang, J.-M., and Tung, C.-H. (2022). MIB2: A web server for metal ion-binding site prediction in protein structures. *Bioinformatics*, 38(18), 4428–4430.

Van Hilten, N., Verwei, N., Methorst, J., Nase, C., Bernatavicius, A., and Risselada, H. J. (2024). PMIpred: A physics-informed web server for quantitative protein–membrane interaction prediction. *Bioinformatics*, 40(2).

Jumper, J., Evans, R., Pritzel, A. et al. Highly accurate protein structure prediction with AlphaFold. Nature 596, 583–589 (2021).

Meng EC, Goddard TD, Pettersen EF, Couch GS, Pearson ZJ, Morris JH, Ferrin TE. Protein Sci. 2023 Nov;32(11):e4792.

De Magistris P, Tatarek-Nossol M, Dewor M, Antonin W. A self-inhibitory interaction within Nup155 and membrane binding are required for nuclear pore complex formation. J Cell Sci. 2018 Jan 4;131(1):jcs208538